International Journal of Biological Macromolecules 363 (2026) 152160

Contents lists available at ScienceDirect

International Journal of Biological Macromolecules

journal homepage: www.elsevier.com/locate/ijbiomac

Direct powder extrusion 3D printing of a polyhydroxybutyrate-based dual-release drug delivery device for dental therapy

Costanza Fratini [a], Matteo Grandoni [a], Tania Vanzolini [a], Annalisa Aluigi [a], Mattia Tiboni [a], Luca Casettari [a,*]

[a] Department of Biomolecular Sciences, School of Pharmacy, University of Urbino Carlo Bo, Via Ca le Suore 2, 61029, Urbino, PU, Italy

ARTICLE INFO

Keywords:
Direct powder extrusion
3D printing
PHB
Additive manufacturing
Material processing

ABSTRACT

This study investigates the processability of polyhydroxybutyrate (PHB) in different physical forms (i.e., powder, pellets, and granules) using direct powder extrusion (DPE) 3D printing (3DP), a technique that enables the direct use of raw materials without prior filament fabrication. The raw materials were thoroughly characterized with respect to their thermal properties to evaluate their suitability for additive manufacturing application. Two DPE 3D printers employing distinct extrusion-driven mechanisms were used to enable a comparative evaluation under identical material conditions. Following printing, the resulting scaffolds were assessed in terms of their thermal, chemical and morphological characteristics to determine the feasibility and performance of each material form within the DPE 3D-printing process. In the second phase of the work, the potential of DPE to fabricate a functional PHB-based dental device enabling dual drug release (i.e., immediate and extended) was investigated. This was achieved by optimizing the printed geometry to incorporate a hydrophilic gel reservoir for burst release. Benzydamine hydrochloride, a non-steroidal anti-inflammatory drug with anti-inflammatory and antimicrobial properties, was selected as the model drug due to its compatibility with PHB processing temperatures (~160 °C). The drug-loaded devices were successfully printed and evaluated through in vitro release studies and antimicrobial testing, confirming both controlled release and biological activity. The findings support the use of PHB and DPE 3DP for the development of customizable, biodegradable drug delivery systems, with promising applications in oral and dental care.

1. Introduction

Polyhydroxybutyrate (PHB) is a biodegradable polymer synthesized by various microorganisms as an intracellular energy storage compound [1–3]. Owing to its biocompatibility, biodegradability, and thermoplastic properties, PHB has garnered significant interest in sustainable material science [4,5]. As the global community increasingly prioritizes environmentally friendly alternatives to petrochemical-derived plastics, PHB emerges as a promising candidate for various applications, ranging from packaging to advanced biomedical devices [5–8]. In particular, it holds the potential to be included in additive manufacturing (AM) techniques such as 3D printing (3DP), representing a significant step towards sustainable and customizable products [9,10]. 3DP has revolutionized the fabrication of complex structures by enabling layer-by-layer construction directly from digital models, offering unparalleled design flexibility, reduced material waste, and the ability to create customized products on demand [11–14]. The integration of PHB into 3DP processes presents an exciting opportunity to develop sustainable and biodegradable products, addressing the growing demand for eco-friendly materials [9,15,16]. PHB's intrinsic features, including high crystallinity, water insolubility, resistance to hydrolytic degradation, thermoplastic properties, and non-toxicity, make it an attractive material for AM applications. Its relatively high melting point (approximately 175 °C) and tensile strength (~40 MPa) enable processing via melt-based 3DP methods [17–19], while its enzyme-mediated biodegradability supports controlled drug release, allowing PHB-based matrices to maintain structural integrity over extended periods and promote gradual diffusion of therapeutic agents through the polymer network [20]. These characteristics have positioned PHB as a suitable candidate for biomedical applications, including drug delivery systems, implants, and scaffolds, where its compatibility with mammalian cells and lack of inflammatory response are critical to clinical success [21–23]. However,

* Corresponding author.
E-mail address: luca.casettari@uniurb.it (L. Casettari).

https://doi.org/10.1016/j.ijbiomac.2026.152160
Received 17 February 2026; Received in revised form 17 April 2026; Accepted 20 April 2026
Available online 22 April 2026

its application in AM is still in its nascent stages, and further research is needed to fully elucidate its processing behaviour, limitations, and optimization strategies.

The present study aims to explore the characterization of PHB in different physical forms (e.g., powder, pellets, and granules) and evaluate its processability using direct powder extrusion (DPE) 3DP technique. DPE enables the direct use of raw materials without prior filament preparation, thereby simplifying the manufacturing process, reducing costs, and broadening the range of printable feedstocks [24,25]. The viability of PHB as a sustainable alternative in the AM context was assessed through a comprehensive investigation of its physicochemical properties, thermal behaviour, and printability. Two different DPE-3D printers employing different extrusion mechanisms were studied in the following work to process PHB in various forms. Thus, allowing for a comparative assessment of instrument performance under identical raw material conditions. This study examines the feasibility of employing powder, pellets, and granules as feeding materials in different DPE printer configurations and evaluates the impact of 3DP processing parameters on the final printed scaffolds. By systematically analysing these factors, this work sets its goal to provide valuable insights into optimizing PHB for AM applications, thereby contributing to the advancement of sustainable polymer technologies in both industrial and biomedical domains. For this purpose, square geometries were printed, adjusting and optimizing printing parameters for each form to achieve desirable printing performance. The resulting 3D-printed scaffolds were then thoroughly characterized through thermal, spectroscopic and morphological analyses. The obtained results were compared with corresponding raw materials to evaluate the post-processing physicochemical integrity of PHB and consequently, to confirm its feasibility for application in the DPE process. Furthermore, this study investigates the use of DPE for the fabrication of a PHB-based dental device designed to provide a dual drug-release profile: immediate and extended. The dual-release behaviour was achieved by engineering the device to incorporate a hydrophilic, drug-loaded gel, whereas geometric optimization ensured that the overall device could be accommodated within the pocket of a dental aligner. Despite their clinical success, clear aligners often act as a physical barrier that alters the oral microenvironment, potentially leading to plaque accumulation, localized gingivitis, and mechanical irritation of the oral mucosa [26]. Conventional pharmacological interventions, such as oral rinses or gels, are often ineffective in this context due to the high turnover of saliva, which rapidly dilutes the active ingredients before they can reach the target tissue. Moreover, the need for frequent reapplications significantly hinders patient compliance. By utilizing a dual-release mechanism—incorporating an immediate-release hydrogel and a sustained-release polyhydroxybutyrate (PHB) matrix—the device aims to maintain therapeutic levels of Benzydamine HCl (Bz HCl) at the point of injury, protecting the drug from salivary washout and providing a "set-and-forget" solution for orthodontic patients. Bz HCl was selected as the model drug due to its dual clinical utility: it effectively mitigates aligner-induced inflammation while simultaneously providing antimicrobial action to suppress pathogen growth [27]. Bz HCl is a non-steroidal anti-inflammatory drug (NSAID) combining anti-inflammatory, analgesic and antimicrobial activities [28] which, thanks to its relatively high melting point (around 160 °C) and good thermal stability, can be processed through DPE at temperatures comparable to those of PHB. The drug was incorporated in the PHB form that was previously identified as the most suitable for the DPE 3DP process. The resulting 3D-printed device was evaluated through in vitro studies to assess drug release and to verify its antimicrobial activity, demonstrating its potential application in dental therapy for maintaining an aseptic and protected oral environment.

2. Materials and methods

2.1. Materials

Poly(3-hydroxybutyrate) (PHB P209, MW > 400 kDa, 50–70% crystallinity, tensile strength 15–20 MPa, 8–15% elongation) in the form of pellets and powder was purchased from Biomer® (Germany). Vinylpyrrolidone-Vinyl acetate copolymer (Kollidon® VA 64) was obtained from BASF (Germany) and Hydroxypropyl Methylcellulose (AFFINISOL™, HPMC HME 15LV and AFFINISOL™, HPMC HME 100LV) from DuPont (USA). Benzydamine hydrochloride (Bz HCl) was kindly obtained from Angelini Pharma spa (Italy). All reagents used were of analytical grade.

2.2. Starting materials and formulation design

2.2.1. Wet granulation

To reduce the volatility and thus improve the flowability of PHB powder inside the printing unit, wet granulation was performed manually. The loose powder was mixed with a binding solution using different agents, such as Kollidon® VA 64 and HPMC 15 LV, at concentrations of 1% and 5% (*w*/w). Solid-to-liquid ratios of 50:50 and 40:60 were evaluated. Tested conditions are shown in Table 1. Mixing was carried out with a mortar and pestle until the powder was fully wetted. The resulting paste was sieved (25 mesh / 0.71 mm), and the obtained granules were air-dried at room temperature (RT) for 24 h.

2.2.2. Preparation of drug-loaded PHB formulations

Granulate F5 and the free PHB powder were also loaded with benzydamine hydrochloride (Bz HCl). In both cases, Bz HCl was incorporated at concentration of 1.5% (*w*/w), selected according to literature data that demonstrated the drug's antiseptic activity at these concentrations [29]. Wet granulation was performed following the same procedure described in Section 2.2.1., while the physical powder blend was obtained through automated mixing with a Galena Top system (Ataena, Italy) for 15 min.

2.2.3. Preparation of the gel containing benzydamine hydrochloride

A gel formulation containing HPMC 100LV and Bz HCl was prepared to provide immediate antiseptic effect, thus aiming for a dual drug release profile system. The formulation was prepared by dissolving HPMC (6% *w*/w) and benzydamine hydrochloride (1.5% w/w) in distilled water under mechanical stirring (400 rpm) until completely dissolved.

2.3. Starting materials and drug-loaded formulations processability at the 3D printer

The processability of PHB in the form of free powder, pellets, and granules was evaluated using Additive Manufacturing (AM). For preliminary 3D printing processing purposes, a square-shaped scaffold (15 × 15 × 5 mm) was designed with Tinkercad® (Autodesk Inc., USA) (Fig. 1-A) and printed using two different 3D printers: Tumaker NX Pro

Table 1
Binding agents and solid-to-liquid ratios studied for wet granulation of PHB powder.

Formulation	Binding agent (% *w*/w)	Solid-to-liquid ratio
F1	Kollidon® VA 64 (1%)	50:50
F2	Kollidon® VA 64 (5%)	
F3	HPMC 15 LV (1%)	
F4	HPMC 15 LV (5%)	
F5	Kollidon® VA 64 (1%)	40:60
F6	Kollidon® VA 64 (5%)	
F7	HPMC 15 LV (1%)	
F8	HPMC 15 LV (5%)	

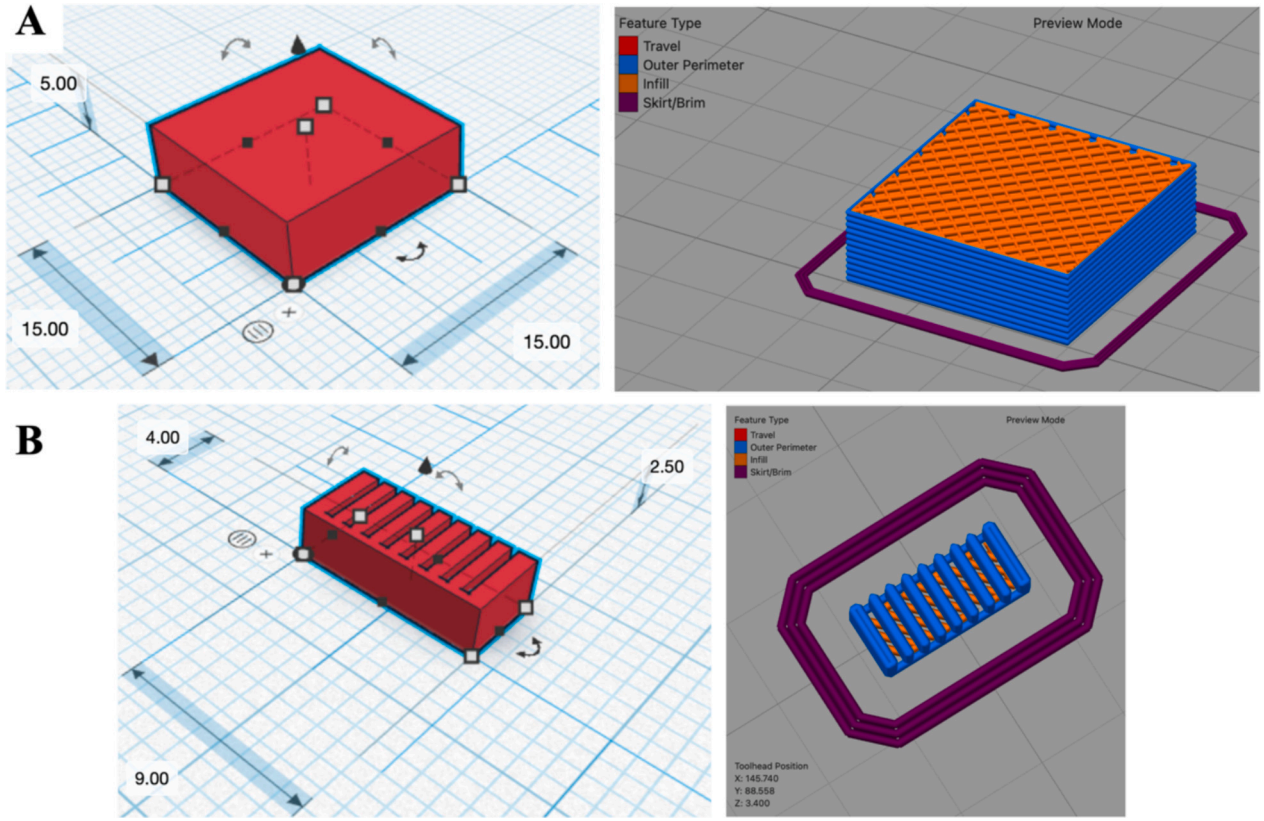

Fig. 1. A) CAD design of a square-shaped scaffold (15 × 15 × 5 mm) (on the left) and printing preview of the CAD design after slicing (on the right); B) CAD design of the rectangular-shaped device (9 × 4 × 2.5 mm) (on the left) and printing preview of the CAD design after slicing (on the right).

(Indart3D, Spain) and BIOX (Cellink, Sweden). Both printers employ the direct powder extrusion (DPE) technique. The Tumaker uses a rotating screw barrel for extrusion, while the BIOX employs air pressure to extrude the molten material from a steel cartridge. Due to different extrusion procedures, the critical operating parameters varied between the two 3D printers and are listed below:

Printing setup (Tumaker):
- Infill: 50%, grid pattern
- Nozzle: 0.4–0.2 mm
- Printhead temperature: 180–200 °C
- Bed temperature: 110–120 °C
- Extrusion multiplier: 0.1–3

Printing setup (BIOX):
- Infill: 50%, grid pattern
- Nozzle: 0.4–0.3 mm
- Printhead temperature: 160–185 °C
- Bed temperature: 65 °C
- Printing pressure: 70–350 kPa
- Printing speed: 3–5 mm/s

2.3.1. Modelling and 3D printing of a dual drug release device

After selecting the most optimal raw starting material and printing setups according to the printer employed, drug-loaded formulations (see Section 2.2.2) were implemented to develop a 3D-printed device with antiseptic properties that could fit into the lateral pocket of a dental aligner (Donatello Aligners, 3D Objects & Data Software SA, Switzerland). A rectangular-shaped scaffold (9 × 4 × 2.5 mm) was designed with Tinkercad® (Autodesk Inc., USA) and provided with a grid design to host the preformulated Bz HCl-loaded gel. The Computer Aided Design (CAD) is illustrated in Fig. 1-B and was further developed via DPE-3DP.

2.4. Pre-processing and post-processing solid-state characterization

2.4.1. Differential scanning calorimetry (DSC)

The thermal profile of PHB in the form of powder, pellets and granules and of the 3D-printed scaffolds was investigated through DSC (DSC 6000, Perkin Elmer, USA). Specifically, approximately 5 mg of sample were placed in aluminium pans and heated up from 25 °C to 250 °C at 10 °C/min. Nitrogen flow rate was kept at 30 mL/min. Additionally, a two-cycle DSC analysis was carried out on the raw materials to mimic the 3D printing process. After the first heating cycle, the sample was cooled from 250 °C to 25 °C at 20 °C/min and subsequently underwent a second heating ramp at 10 °C/min. Data collection and analysis was performed using Pyris Manager software (Perkin Elmer, USA).

2.4.2. Thermogravimetric analysis (TGA) and TGA coupled with Fourier-transform infrared spectroscopy (FTIR)

To evaluate the degradation of the various forms of PHB and of the resulting 3D-printed scaffolds, TGA analysis was run from 25 °C to 550 °C, at a speed rate of 10 °C/min, using nitrogen flow at 30 mL/min. Data collection and analysis was performed using Pyris Manager software (Perkin Elmer, USA).

For the raw starting materials, TGA analysis was also coupled with Fourier-Transform infrared spectroscopy (FTIR) to study the composition of the fumes produced during thermal degradation. Nitrogen flow rate was set at 70 mL/min and spectra were collected in transmittance (%) from 4000 to 400 cm^{-1} with a resolution of 64 cm^{-1} for the entire duration of the analysis.

2.4.3. Fourier-transform infrared spectroscopy (FTIR)

Raw PHB and 3D-printed scaffolds were also characterized by FTIR (ATR-FTIR, Spectrum Two, Perkin Elmer, USA). Transmittance (%) was recorded in the wavelength interval of 4000–400 cm^{-1} with a resolution of 64 cm^{-1}. Air was used as the background for each analysis.

2.4.4. Powder X-ray diffraction (PXRD)

The crystalline structure of the raw starting materials and 3D-printed scaffolds was investigated using a benchtop diffractometer (Miniflex, Rigaku, Tokyo, Japan) with Cu-Kα radiation (λ = 1.5418 Å) source and a D/teX Ultra2 detector. All the measurements were conducted in the 2θ range of 5–50° with a step size of 0.01° and a scan speed of 5°/min.

2.4.5. Scanning electron microscopy (SEM)

The morphology of the raw materials and final 3D-printed scaffolds was examined with a scanning electron microscope (SEM JEOL IT200LA, JEOL, Japan). Imaging was performed in low-vacuum mode under a specimen chamber pressure of 10 Pa, with an acceleration voltage of 20.0 kV and a standard probe current (Std-PC). Magnifications ranged from 30× to 1500×, while the working distance was maintained at 10.0 mm to ensure optimal resolution and depth of field.

2.5. Drug content and uniformity of Bz HCl-loaded formulations

To evaluate the effective drug loading of Bz HCl in the prepared formulations and assess its homogenous distribution, High Performance Liquid Chromatography (HPLC) coupled with UV–Vis analysis was carried out.

Each sample (about 40 mg) was put into dialysis bags (cut-off 12–14 kDa MWCO) and soaked in 30 mL of phosphate buffered saline (PBS, pH 7.4) under stirring (200 rpm). At 4 and 24 h time points, 1 mL sample was collected and placed into vials suitable for UV-HPLC (Agilent 1260 Infinity II, Agilent, USA). The analysis was performed at room temperature (RT) using an Agilent Zorbax Eclipse Plus C18, 150 × 4.6 mm, 5 μm column (Agilent, USA). 0.5% (v/v) formic acid (FA) in water and methanol (40:60) were selected as mobile phases, setting the flow rate at 1 mL/min and the injection volume at 20 μL. The detection signal was recorded at 307 nm. A calibration curve in PBS (pH 7.4) was also performed, and linearity was demonstrated over the interval of 3.9–50 μg/mL with an R^2 value equal to 0.9999.

Regarding the HPMC gel, the uniformity assay was also conducted by FTIR spectroscopy (procedure detailed in Section 2.4.3). The preformulated gel was spread on a petri dish and let dry overnight at RT. Then three random samples were collected and analysed.

2.6. In vitro drug release

The release profile of Bz HCl from the HPMC gel and PHB-based matrix was studied in triplicate through a dissolution study. For this purpose, each sample was placed in 5 mL of PBS (pH 7.4) under stirring at 37 °C. The volume of the release medium was calculated to maintain sink conditions, defined as at least 3–5-fold excess relative to the volume required for complete dissolution of the total drug load, thereby preventing saturation-limited release. Aliquots (200 μL) were withdrawn at specified timepoints (5; 10; 15; 30; 60; 90; 120; 240 and 360 min for the gel, while 0.5; 1; 2; 4; 6; 24; 48; 72; 144 h for the PHB matrix), and replaced with an equal volume of fresh PBS. The collected samples were analysed via UV-HPLC to quantify the amount of Bz HCl released, employing the same analytical method described in Section 2.5.

2.7. In vitro antimicrobial activity

The antimicrobial activity of the final Bz HCl-loaded 3D-printed device was measured by the disc diffusion test, through the evaluation of the zone of inhibition. Common oral pathogens, *Staphylococcus aureus* (ATCC 43387) and *Candida albicans* (ATCC 10231) were selected as targets and were maintained on Luria–Bertani (LB; Sigma-Aldrich) and Potato Dextrose Agar (PDA; Sigma-Aldrich) plates, respectively. 3D-printed devices, both Bz HCl-loaded and unloaded (negative control), were sterilized by UV irradiation under a laminar-flow hood. Antimicrobial activity was evaluated using a modified agar disk diffusion protocol. Briefly, microbial cultures were inoculated into LB broth and incubated overnight at 37 °C under stirring. The following day, microbial growth was detected by spectrophotometric analysis at 600 nm (Optical Density or OD_{600}), and the microbial suspension was adjusted to a 0.5 McFarland standard. A sterile swab was immersed in the standardized suspensions and used to uniformly seed the surface of agar plates (LB for *S. aureus*; PDA for *C. albicans*).

After brief drying, devices were placed centrally on the agar surface, ensuring that the devices were in full contact with the agar surface. Plates were incubated at 37 °C. After 24 h microbial growth was examined, and inhibition zones were manually measured with a ruler.

2.8. Statistical analysis

All the analyses were carried out in triplicate and results are shown as mean ± standard deviation (SD). Data from all experiments were analysed using a *t*-test, and differences were considered significant for $p < 0.05$.

3. Results and discussion

3.1. Wet granulation

Due to its high volatility and poor flowability, PHB powder presented some drawbacks for direct processing. To address these limitations, a wet granulation approach was employed. Binding solutions were prepared using various agents and concentrations, as detailed in Table 1. Initially, a solid-to-liquid ratio of 50:50 was tested (formulations F1–F4). While this ratio facilitated homogeneous mixing, it did not yield a sufficiently cohesive paste. Consequently, the liquid content was increased, and a 40:60 solid-to-liquid ratio was evaluated (formulations F5–F8). This adjustment resulted in the formation of a cohesive and uniformly wetted paste, with complete dispersion of the powder particles within the liquid phase (Fig. 2, Panel I-A). Based on these observations, the 40:60 ratio was selected as the desired condition for PHB granulation. The resulting granules were air-dried at RT for 24 h. Post-drying analysis revealed that formulations F5 and F8 produced dry granules with minimal residual loose powder (Fig. 2, Panel I—B). Therefore, F5 and F8 were identified as the most promising candidates for subsequent processability studies via direct powder extrusion 3D Printing (DPE-3DP). Fig. 2, panel II represents the granules obtained from the selected formulations after sieving through a 25 mesh (0.71 mm), both prior to and after 24 h drying at RT.

For the sake of clarity, this study distinguishes between pellets and granules based on their formation and morphology. Pellets refer to the original industrial raw material (specifications reported in Section 2.1), characterized by a dense, cylindrical shape (~ 3 mm) typically obtained through thermal fusion methods such as melt extrusion. In contrast, granules represent an intermediate form produced, as previously described, from the PHB powder via a cold process, where the powder is wetted with a liquid binder at room temperature to create porous agglomerates (~ 0.5–1 mm). This distinction is crucial for the Direct Powder Extrusion (DPE) process, as the different particle sizes and surface area-to-volume ratios significantly influence feeding consistency and melting behaviour within the printer's hopper. While the larger, uniform pellets provide predictable flow, the smaller, irregular granules offer a different surface chemistry that can affect the transition from a solid state to a melt during 3D printing.

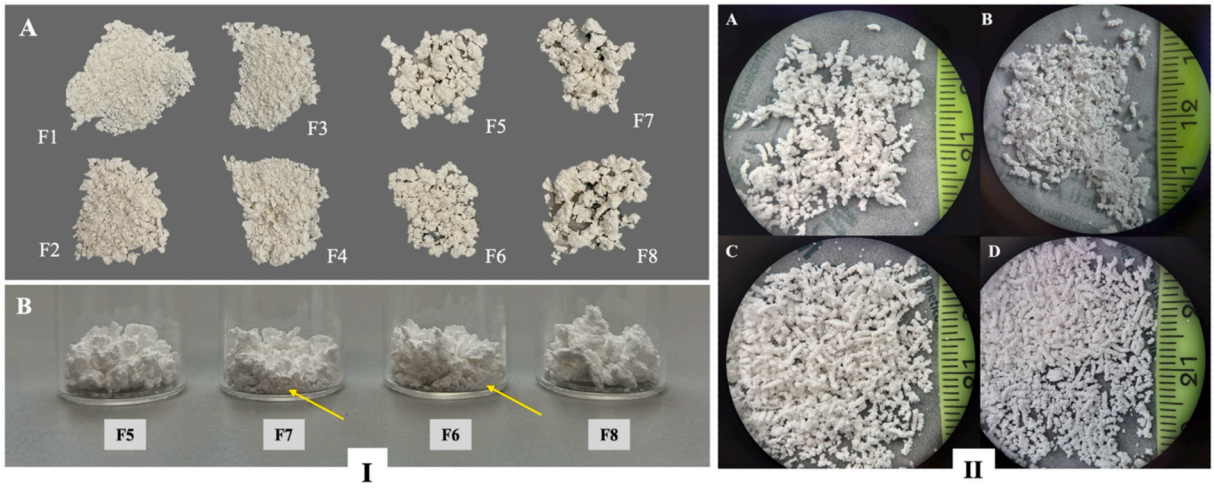

Fig. 2. Panel I: Preliminary test of wet granulation of PHB powder using different binding agents at different concentrations and different solid-to-liquid ratios (A); preliminary 24 h-dry granules using a 40:60 solid-to-liquid ratio and different binding agents at different concentrations. F7 and F6 show the highest amount of loose powder after drying (B). Panel II: images of F5 and F8 granules before (A and C) and after (B and D) 24 h air-drying at the optical microscope (magnification 7×).

3.2. PHB powder, pellets and granules processability at the 3D printer

The processability of PHB in the form of free powder, pellets, and granules (F5 and F8) was systematically evaluated via additive manufacturing (AM), specifically through the DPE-3DP technique. Unlike fused deposition modelling (FDM), DPE enables the direct processing of raw materials or material blends without the prerequisite of filament fabrication [30,31].

The present study builds upon and extends previously published work on PHB processing by melt-based additive manufacturing. Prior studies consistently reported that PHB is challenging to process due to its narrow thermal processing window, high crystallinity, and susceptibility to thermal degradation and warpage, particularly when conventional FDM is employed [4,10,32].

In this study, DPE was implemented using two different 3DP systems. Although both operate on the same fundamental principle of blend melting and extrusion, they differ in their extrusion mechanisms: the Tumaker printer utilizes a barrel screw system, whereas the BIOX printer employs pneumatic (air pressure-based) extrusion. These differences necessitate the monitoring and adjustment of specific operational parameters, such as the extrusion multiplier (EM) and pressure.

EM is a critical parameter that controls the volume of material extruded through the nozzle. Defined as a percentage (with 100% corresponding to a value of 1), the EM serves as a flow rate coefficient, allowing the fine-tuning of material output to mitigate issues such as over or under-extrusion [33,34]. This adjustment is essential to achieve optimal 3DP quality across different materials and conditions.

Conversely, in the BIOX system which doesn't involve a barrel screw, the EM is not a configurable parameter. Instead, extrusion control is achieved solely by adjusting the pneumatic pressure at a given operating temperature. This pressure modulation governs the material flow rate, enabling optimization of extrusion and minimizing defects.

Pellets: In the Tumaker system, optimal temperature for PHB pellets extrusion was set at 182 °C, however over-extrusion occurred, which could be mitigated by reducing the EM to 0.4 and the nozzle diameter from 0.4 mm to 0.2 mm (Fig. 3, panel I, A and B). Slight increases in temperature (e.g., 185 °C) significantly reduced the viscosity of the molten PHB, resulting in unstable flow (Fig. 3, panel I, C and D). Bed adhesion was poor and required the use of a polypropylene (PP) adhesion sheet. In the BIOX system, pellets at 160 °C showed pronounced over-extrusion due to the inherently low viscosity of molten PHB (Fig. 3, panel I, E and F). Lowering the extrusion temperature to 155 °C led to incomplete melting and poor flow, while pressure adjustments failed to solve the issue. As with the Tumaker, a PP adhesion sheet was necessary to improve bed adhesion.

Powder: When processed in the Tumaker (200 °C), PHB powder produced extruded strands with enhanced plasticity compared to those from pellets, which were more brittle and rougher. However, limited flowability within the barrel screw led to insufficient `feeding and under-extrusion phenomena (Fig. 3, panel II, A and B). Increasing the EM from 1 to 3 did not improve the flow. Bed adhesion was weak but could be improved by increasing temperature (120 °C) and using a PP adhesion sheet. In the BIOX system, powder extrusion (175 °C) showed better control over the amount of material dispensed (Fig. 3, panel II, C). Nonetheless, strong adhesion of the powder to the cartridge walls disrupted flow consistency, leading to air extrusion and compromised print quality (Fig. 3, panel II, D). The limited bed temperature (max 65 °C) caused premature detachment of the printed material, and the PP adhesion sheet failed in adhesion improvement.

Granules (*F5*): In the Tumaker system, F5 yielded extrudates with a smooth surface, high plasticity, and flexibility, without signs of brittleness. The granules exhibited good flowability and consistent feeding, resulting in reliable and reproducible prints at 200 °C (Fig. 3, panel IV, A and B). Bed adhesion was improved compared to pure PHB powder. In the BIOX system, F5 allowed for good control over extrusion at 175 °C (Fig. 3, panel IV, C) while reduced adhesion to the cartridge walls minimized air entrapment, although air bubbles were still present in the extruded strands (Fig. 3, panel IV, D). Bed adhesion was better compared to the free powder but remained suboptimal due to temperature limitations with PP adhesion sheet providing only marginal improvement.

Granules (*F8*): F8 processed in the Tumaker printer at 200 °C produced extrudates with good plasticity, and flexibility, along with increased stickiness compared to F5. Feeding and flowability were efficient, and extrusion was stable (Fig. 3, panel III, A and B). Minor over-extrusion phenomena were observed but could be corrected by reducing the EM. Bed adhesion was significantly improved over both powder and F5 granules. In the BIOX system, F8 granules showed poor control over extrusion at 175 °C (Fig. 3, panel III, C and E). The material's high stickiness, attributed to the presence of hydroxypropyl methylcellulose (HPMC), led to strong adhesion to the cartridge walls, causing air entrapment and inconsistent flow (Fig. 3, panel III, D and F). Despite these issues, bed adhesion was improved related to powder and F5.

Air entrapment was generally observed in strands extruded using the BIOX system, particularly in cases where high material stickiness compromised the flowability of the molten PHB. This impaired flow

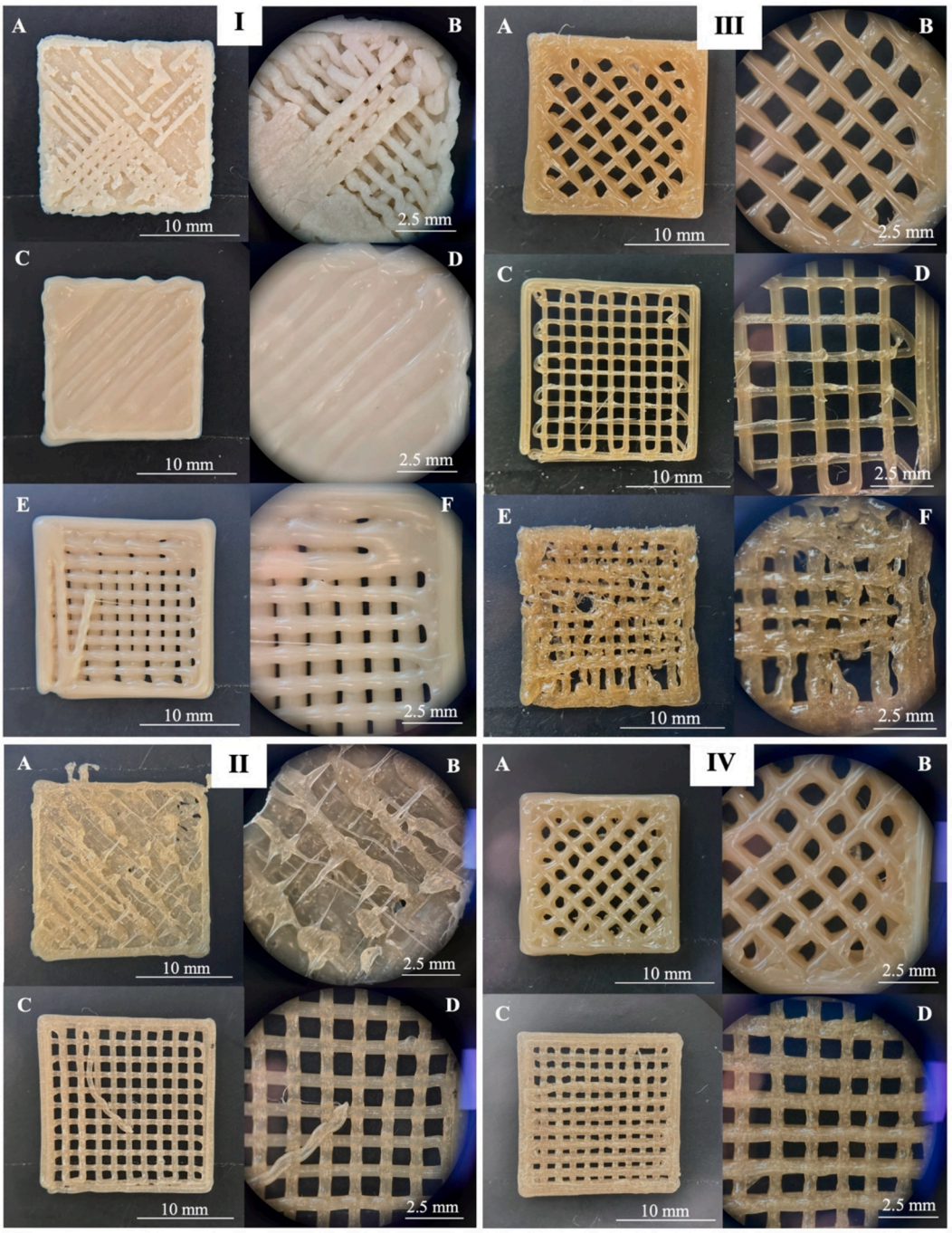

Fig. 3. Images of the 3D-printed scaffolds at the optical microscope (7× and 25× magnification) obtained from drug-free PHB: pellets (panel I), powder (panel II), F8 granules (panel III), and F5 granules (panel IV). Panel I: Scaffolds 3D-printed using Tumaker (A-D) and using BIOX (*E*-F). Panel II: Scaffolds 3D-printed using Tumaker (A-B) and using BIOX (C-D). Panel III: Scaffolds 3D-printed using Tumaker (A-B) and using BIOX (C-F). Panel IV: Scaffolds 3D-printed using Tumaker (A-B) and using BIOX (C-D).

behaviour led to the extrusion of air, which disrupted the continuity and quality of the printing process. Additionally, a notable difference in processing temperature, approximately 20 °C, was observed between the Tumaker and BIOX systems. This discrepancy may be attributed to a more precise thermal regulation of the steel cartridge in the BIOX printer. In fact, the processing temperatures recorded in the BIOX system are closely aligned with the melting temperature (T_m) determined via differential scanning calorimetry (DSC), as discussed in Section 3.3.1.

A summary of the processing outcomes for PHB in its various physical forms across the two DPE-equipped 3D printers is provided in Table 2.

In agreement with previously published literature [21,35], our results confirm that careful control of processing parameters is essential to preserve structural integrity and reproducibility during printing of PHB. At the same time, the retention of solid-state characteristics observed in our system and reported in the following sections, are consistent with earlier findings describing the intrinsic thermal robustness of PHB when appropriately handled [5,17].

A key distinction between the present work and most previously reported PHB 3D-printing studies lies in the manufacturing approach. Most of the literature relies on filament-based FDM, which requires an additional extrusion step and introduces a cumulative thermal history

Table 2
Summary of printing conditions and outcomes observed for the different PHB forms (pellets, powder and granules F5 and F8) at the two DPE 3D printers.

Feedstock	Characteristics	Tumaker NX Pro	BIOX
Pellets	Operating parameters	Printing temperature: 182 °C Nozzle: 0.2 mm EM: 0.4 Bed temperature: 110 °C	Printing temperature: 160 °C Nozzle: 0.2 mm Pressure: 85 kPa Bed temperature: 65 °C (max)
	Flowability/ feeding	Challenging due to low viscosity, poor flow control	Challenging due to low viscosity, poor flow control
	Extruded strands quality	Brittle and rough or too fluid and smooth	Brittle and rough or too fluid and smooth
	Extrusion/ printing	Pronounced over-extrusion, incomplete melting at lower temperatures	Pronounced over-extrusion, incomplete melting at lower temperatures
	Bed adhesion	Weak, manageable with temperature increase and PP adhesion sheet	Very weak, slight increase with PP adhesion sheet
Powder	Operating parameters	Printing temperature: 200 °C Nozzle: 0.4 mm EM: from 1 to 3 Bed temperature: 120 °C	Printing temperature: 175 °C Nozzle: 0.4 mm Pressure: 350 kPa Bed temperature: 65 °C (max)
	Flowability/ feeding	Limited flowability, insufficient feeding,	Good control but disrupted by adhesion to cartridge walls
	Extruded strands quality	More plastic and flexible compared to PHB pellets	More plastic and flexible compared to PHB pellets
	Extrusion/ printing	Under-extrusion, no improvement with increased EM	Good extrusion with air bubbles
	Bed adhesion	Weak, manageable with temperature increase and PP adhesion sheet	Premature detachment, PP adhesion sheet ineffective
F5	Operating parameters	Printing temperature: 200 °C Nozzle: 0.4 mm EM: 0.5 Bed temperature: 120 °C	Printing temperature: 175 °C Nozzle: 0.4 mm Pressure: 280 kPa Bed temperature: 65 °C (max)
	Flowability/ feeding	Efficient feeding, good flowability	Good control, reduced adhesion to cartridge walls
	Extruded strands quality	Smooth, plastic, flexible without brittleness	Smooth, plastic, flexible without brittleness
	Extrusion/ printing	Consistent extrusion, reliable printing outcomes	Consistent extrusion, reliable printing outcomes, air bubbles
	Bed adhesion	Improved related to pure PHB powder, enhanced by PP adhesion sheet and higher temperatures	Improved relative to free powder, slightly enhanced by PP adhesion sheet
F8	Operating parameters	Printing temperature: 200 °C Nozzle: 0.4 mm EM: 0.3 Bed temperature: 110 °C	Printing temperature: 170 °C Nozzle: 0.4 mm Pressure: 220 kPa up to 600 kPa Bed temperature: 65 °C (max)
	Flowability/ feeding	Efficient feeding, good flowability	Poor control, high adhesion to cartridge walls
	Extruded strands quality	Smooth, flexible, increased stickiness	Pronounced stickiness due to HPMC, air bubbles
	Extrusion/ printing	Stable extrusion, minor over-extrusion	Significant air entrapment, inconsistent flow
		corrected by adjusting EM	
	Bed adhesion	Improved compared to pure PHB powder and F5 granules	Improved compared to pure PHB powder and F5 granules

that may promote polymer degradation or crystallinity changes. In contrast, the use of DPE enables more direct processing of PHB, reducing thermal exposure prior to printing. The preserved thermal behaviour and consistent print quality observed in this study suggest that DPE may better maintain the intrinsic properties of PHB compared to filament-based methods, while also offering greater flexibility for rapid material screening and device customization.

3.2.1. *Drug-loaded formulations processability at the 3D printer*

Based on the observations and processability outcomes, granulate F5 and the free PHB powder were selected as the most suitable PHB forms for processing via DPE through Tumaker and BIOX printers respectively. Once the printability of the drug-loaded formulations was verified (Fig. 4, panel I-II), these were subsequently employed as starting materials for the fabrication of a customized device for dental application (Fig. 4, panel III).

Granulate F5: In the Tumaker system, granules showed a better flowability than powder and produced more plastic and flexible extrudates. Particularly, among the granules, F5 proved to be the optimal feedstock owing to minor over-extrusion phenomena and improved printing outcomes compared to F8. The drug-loading did not result in significant changes in both flowability and extrusion temperature that remained unchanged (~195 °C). Likewise, the favourable properties of the extruded strand, including the high plasticity, were preserved. Furthermore, an improved bed adhesion was observed.

Powder: Based on previous observations, in the BIOX system, PHB powder was preferred. Compared to granules, powder allowed a better control over the extrusion and yielded extrudates with enhanced plasticity. Also in this case, no notable variations in printing parameters (printing temperature: 175 °C; pressure: 200–300 kPa) were observed after the drug incorporation. Slight over-extrusion occurred but could be corrected by reducing the nozzle diameter from 0.4 to 0.2 mm. The bed adhesion was improved compared to free powder.

A summary of the processing outcomes for drug-loaded PHB formulations across the two DPE 3D printers is provided in Table 3.

Beyond processing considerations, most PHB 3D-printing studies focus on mechanical performance or scaffold fabrication for tissue and biomedical engineering applications [22,23,36]. The present work expands this scope by demonstrating the feasibility of PHB-based in additive manufacturing for sustained, localized drug delivery highlighting the potential of PHB not only as a structural biomaterial but also as a functional matrix for controlled release applications.

3.3. *Pre-processing and post-processing solid-state characterization*

3.3.1. *Differential scanning calorimetry (DSC)*

DSC analyses were performed to assess the thermal behaviour of the raw materials and 3D-printed scaffolds. Particularly, a two cycle DSC analysis was conducted on raw materials to simulate the 3D-printing process, comparing the results obtained with those of 3D-printed scaffolds. The melting temperature (T_m), melting enthalpy (ΔH_m), cold crystallization temperature (T_{cc}), and cold crystallization enthalpy (ΔH_{cc}) were obtained from DSC scans, while the degree of crystallinity (X_c) was calculated using the measured enthalpy values according to Eq. (1), where ΔH_0 stands for the theoretical melting enthalpy for 100% crystalline PHB (146 J/g).

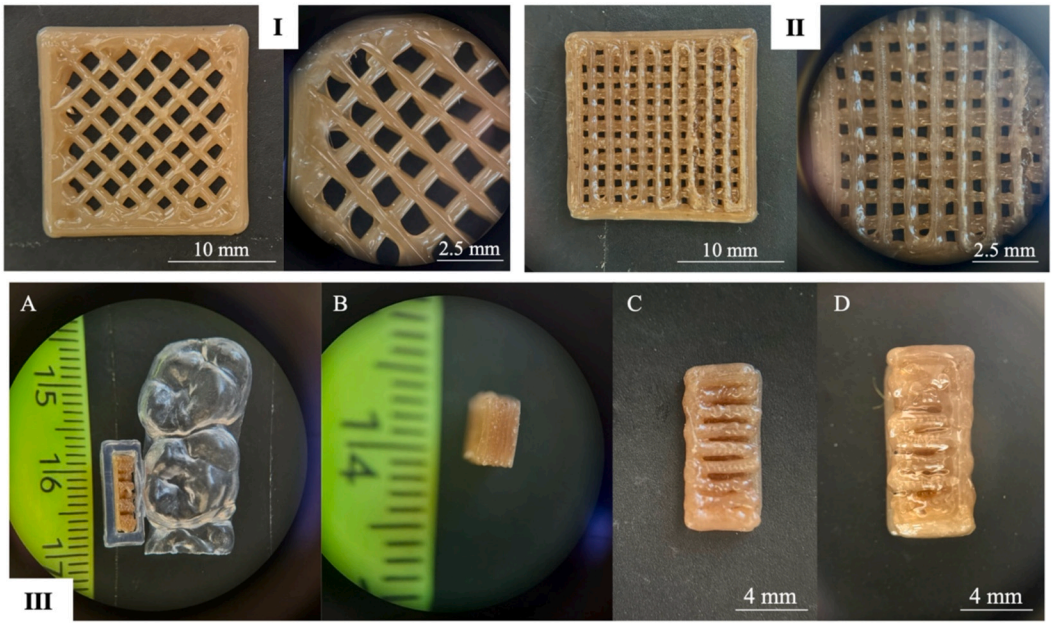

Fig. 4. Images of the drug loaded 3D-printed scaffolds (panel I and II) and 3D-printed device (panel III) at the optical microscope (7× and 25× magnification). Panel I: Scaffolds 3D-printed using Tumaker from drug-loaded F5 granules. Panel II: Scaffolds 3D-printed using BIOX from physical powder blend. Panel III: 3D-printed device within the pocket of the dental aligner (A); side view of the device (B); top view of the unloaded device (C); top view of the device loaded with the gel (D).

Table 3
Summary of printing conditions and outcomes observed for the Bz HCl-loaded PHB formulations at the two DPE 3D printers.

Feedstock	Characteristics	Tumaker NX Pro	BIOX
F5 + Bz HCl	Operating parameters	Printing temperature: 195 °C Nozzle: 0.2 mm EM: 0.7 Bed temperature: 110 °C	/
	Flowability/ feeding	Efficient feeding, good flowability	
	Extruded strands quality	Smooth, plastic, flexible without brittleness	
	Extrusion/ printing	Consistent extrusion, reliable printing outcomes	
	Bed adhesion	Improved compared to unloaded F5 granules	
Powder + Bz HCl	Operating parameters	/	Printing temperature: 175 °C Nozzle: 0.2 mm Pressure: 250 kPa Bed temperature: 65 °C (max)
	Flowability/ feeding		Good control but disrupted by adhesion to cartridge walls
	Extruded strands quality		Plastic and flexible
	Extrusion/ printing		Good extrusion, minor over-extrusion corrected by adjusting the nozzle diameter
	Bed adhesion		Improved related to free powder

$$X_c\ (\%) = [(\Delta H_m - \Delta H_{cc})/\Delta H_0\,] \times 100 \quad (1)$$

The obtained results for each sample are summarized in Table 4.

Raw Materials: DSC thermograms revealed significant differences between PHB pellets and the other PHB forms (Fig. 5, panel I-A). During the first heating ramp, powder and granules showed a single endothermic peak related to the characteristic melting of the crystalline fraction of the polymer $T_m = 174.48 \pm 3.10$ [37,38] and subsequently two endothermic peaks at lower temperatures (~ 138 °C and 150 °C) during the second heating stage. This phenomenon can be attributed to a bimodal distribution of crystal size, resulting from changes in molecular weight following random splitting of the long PHB chains [39–41]. Regarding pellets, due to the presence of additives employed during the fabrication process [42], two peaks were observed in the DSC thermograms during both heating scans: a small endothermic peak at lower temperature (~ 58 °C), probably attributed to the melting of additives and the PHB characteristic melting peak, which presented a broadened shape and shifted slightly to a lower temperature compared to the powder and granules ($T_m = 161.27 \pm 2.96$ °C); a common outcome when additives such as plasticizers are present in the sample [39,40]. During the cooling scan, PHB pellets recrystallized, showing a clear exothermic peak. In contrast, granules F5 and F8 did not crystallize on cooling but instead displayed an exothermic peak during the second heating, indicating cold crystallization [43,44] while PHB powder showed both recrystallization during cooling and second heating stage. The different behaviour in the various PHB forms might be explained by the fact that the polymer partially recrystallizes during the cooling and partially during reheating, and the relative amount of polymer recrystallizing in each stage depends on the heating or cooling rate and on the presence of any additives in the observed sample [40,41] as it is the case for pellets and granules F5 and F8 where Kollidon VA 64 and HPMC HME 15LV acted as plasticizers.

Drug and drug-loaded formulations: As reported in Fig. 5, panel I—B and C, Bz HCl showed a characteristic endothermic peak, related to the melting at $T_m = 161.03 \pm 2.47$ [45,46]. Furthermore, no peaks were observed during the cooling and the second heating scans, suggesting that the drug didn't recrystallize after melting. However, after the drug incorporation differences regarding PHB recrystallization and melting were detected. The recrystallization differences and the presence of one single and broader melting peak in the drug-loaded formulations compared to their drug-free counterparts suggested that Bz HCl may also

Table 4
Main thermal properties of the different PHB forms, Bz HCl, and drug-loaded formulations determined by DSC analysis. T_m, T_c, and T_{cc} correspond to the melting, crystallization, and cold crystallization temperatures, respectively; X_c represents the calculated degree of crystallinity.

Sample	1st heating stage	2nd heating stage		Cooling stage	X_c (%)
	T_m (°C)	T_m (°C)	T_{cc} (°C)	T_c (°C)	
PHB pellet	161.27 ± 2.96	150.25 ± 1.75	/	67.64 ± 0.68	44.19 ± 1.72
PHB powder	174.48 ± 3.10	137.99 ± 2.78 152.55 ± 1.27	44.56 ± 1.10	58.32 ± 1.34	54.98 ± 3.19
F5	174.99 ± 1.60	137.09 ± 1.28 152.65 ± 0.71	45.27 ± 1.08 55.35 ± 1.47	/	50.86 ± 2.76
F8	175.60 ± 3.08	137.61 ± 1.74 151.75 ± 3.04	72.08 ± 0.66	/	57.58 ± 3.65
BZ HCl pure drug	161.03 ± 2.47	/	/	/	96.32 ± 2.23
F5 + Bz HCl	175.11 ± 2.97	171.35 ± 0.50	53.48 ± 2.42	85.07 ± 0.90	56.38 ± 1.59
PHB powder + Bz HCl	174.92 ± 1.23	170.8 ± 1.39	49.65 ± 1.60	83.80 ± 1.25	56.74 ± 3.09
F5 @Tumaker	174.54 ± 0.67	/	/	/	50.33 ± 2.90
F5 + Bz HCl @Tumaker	172.84 ± 1.16	/	/	/	50.70 ± 1.77
PHB powder @BIOX	172.46 ± 1.15	/	/	/	52.95 ± 0.89
PHB powder + Bz HCl @BIOX	171.78 ± 1.60	/	/	/	51.15 ± 1.36

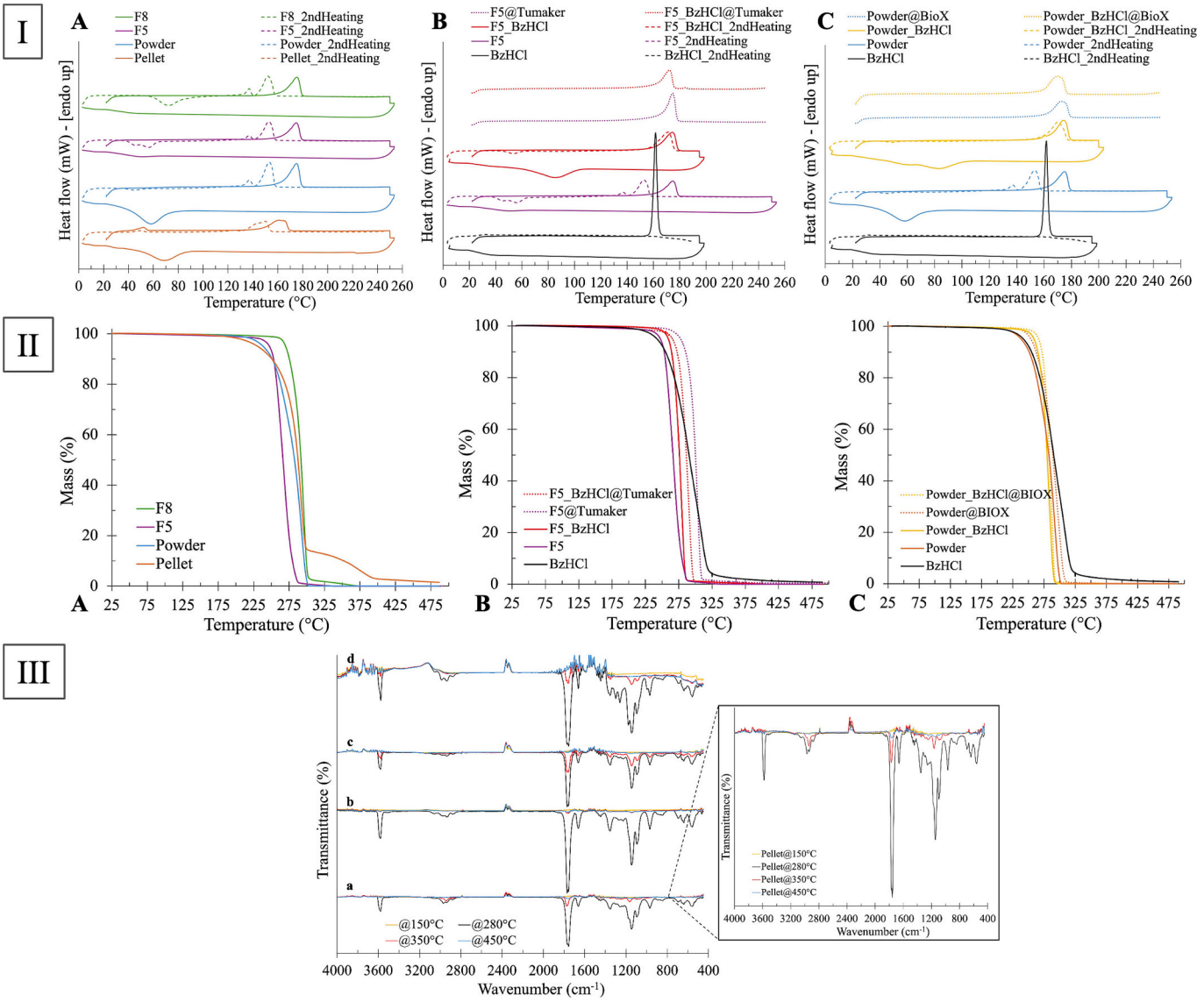

Fig. 5. Panel I: DSC thermograms of raw materials, drug-loaded formulations and 3D-printed scaffolds. PHB pellets, powder and granules(A); drug-loaded and unloaded granulate F5 and corresponding 3D-printed scaffolds (B); drug-loaded and unloaded powder and corresponding 3D-printed scaffolds (C). Panel II: TGA thermograms of raw materials, drug-loaded formulations and 3D-printed scaffolds. PHB pellets, powder and granules (A); drug-loaded and unloaded powder and corresponding 3D-printed scaffolds (B); drug-loaded and unloaded granulate F5 and corresponding 3D-printed scaffolds (C). Panel III: TGA-FTIR analysis of the raw materials, showing FTIR spectra of pellets (a), powder (b), granulate F5 (c) and granulate F8 (d), recorded at relevant temperatures (150, 280, 350 and 450 °C).

act as a plasticizer towards the polymer, as previously described.

3D printed scaffolds: 3D-printed scaffolds, as shown in Fig. 5, panel I—B and C, displayed a single endothermic peak at ~173 °C, and their DSC traces were compared with those obtained for the corresponding raw material. No appreciable shift in melting temperature was observed, consistent with previous studies [47–49] reporting that thermal properties of PHB remain unchanged upon thermal processing.

Among the raw materials, PHB pellets were the only form exhibiting reduced crystallinity, likely due to the presence of additives [50]. In contrast, PHB powder and granules showed crystallinity values of approximately 55–60%, which are typical for this polymer. Granules F5 displayed a slightly lower crystallinity (~50%), possibly reflecting a stronger plasticizing effect of HPMC compared to Kollidon, consistent with the improved granulation performance observed. No significant changes were instead detected after PHB processing in the 3D printer, as the crystallinity of the printed scaffold remained comparable to that of the starting formulations.

3.3.2. Thermogravimetric analysis (TGA) and TGA coupled with Fourier-transform infrared spectroscopy (FTIR)

The thermal stability and the degradation profile of the samples were analysed by TGA. The temperatures corresponding to the maximum degradation rate (T_d) were evaluated through derivative thermogravimetry (DTG) and are listed in Table 5.

Raw materials: TGA curves of the various forms of PHB are depicted in Fig. 5, panel II-A, highlighting differences among the samples. Powder and granules F5 and F8 showed a single weight loss event, which means that the thermal degradation of PHB proceeded exclusively by only one mechanism: a non-radical random chain scission reaction (cis-elimination) [44,51]. Specifically, the thermal decomposition of granules F5 and F8 took place within a narrower range than that of the powder, resulting in complete decomposition of F5 at about 335 °C, whereas the residual mass of F8 at that temperature was about 1.45%. Instead, PHB pellets presented a two-step thermal degradation: the main degradation step ($T_d = 292.57 \pm 2.96$ °C) led to a weight loss of about 86%, while a small degradation event initiated at 320 °C, showing a $T_d = 379.53 \pm 3.41$ °C. The multistep degradation process was attributed to the presence of additives such as plasticizers. The residual mass (about 1.5%) detected after the thermal decomposition of PHB, suggested the presence of non-volatile inorganic particles, such as nucleating agents [40,42].

Considering the differences identified in the TGA profiles of the raw materials, the analysis was coupled with FTIR, examining the fumes produced during thermal degradation. The FTIR spectra recorded at the relevant temperatures are shown in Fig. 5, panel III. PHB underwent thermal degradation starting at approximately 200–230 °C, leading to the generation of several degradation products, including crotonic acid, crotonic acid dimers and trimers, linear oligomers with terminal crotonate groups [52,53], propene and 2-propenyl butanoate [54]. Accordingly, the most prominent peaks were detected in the FTIR spectra recorded at 280 °C and they were conserved across all samples: absorptions at 3580 cm^{-1} and 968 cm^{-1} were attributed to the -OH vibration in the carboxylic group, multiplet band observed within the range of 3056 to 2870 cm^{-1} related to CH_3 and CH_2 groups stretching vibrations, a double peak at 1770 and 1758 cm^{-1} corresponding to carbonyl (C=O) stretching vibration in unsaturated esters and unsaturated carboxyl acids, the band at 1662 cm^{-1} of C=C stretching, the signal at 1354 cm^{-1} related to the bending vibration of CH_3 and CH_2 groups, and the peaks between 1146 and 1092 cm^{-1} due to C—O stretching in esters [54–56]. In the spectra acquired at higher temperatures (350 and 450 °C), detectable signals were observed exclusively for pellets and granules, in contrast to the powder which is free of additives. Specifically, a peak at 2942 cm^{-1} (CH_2 stretching vibration) and a distinct band at 1772 cm^{-1} (C=O stretching) were detected for pellets in the FTIR spectrum at 350 °C, while, at the same temperature, the spectra of granules were characterized by prominent signals at 3580 cm^{-1} (-OH stretching) and at 1758 cm^{-1} (C=O stretching), as well as by bands in the 1358–968 cm^{-1} and 890–482 cm^{-1} regions. A band at 1662 cm^{-1}, attributed to C=C stretching [54] was also observed only in F5 spectrum. Furthermore, pellets also displayed weak bands at 1758 cm^{-1} and 1150 cm^{-1} in the spectrum recorded at 450 °C.

Drug and drug-loaded formulations: As shown in Fig. 5, panel II-B and C, a similar degradation trend was observed for the drug-loaded samples, with the only difference being a slightly narrower degradation temperature range. Therefore, the addition of the drug, which showed a single thermal weight-loss with a $T_d = 308.92 \pm 2.47$ °C, didn't result in any relevant variations.

3D-printed scaffolds: TGA curves are reported in Fig. 5, panel II-B and C. The 3D-printed scaffolds exhibited a thermal degradation profile comparable to those of the corresponding PHB forms. No significant differences were detected, in agreement with literature reports [47,48] indicating that PHB thermal processing didn't substantially affect its thermal properties, such as T_d.

Table 5
Temperatures at maximum degradation rate (T_d) determined by DTG analysis.

Sample	T_d (°C)
PHB pellet	292.57 ± 2.96
PHB powder	291.89 ± 1.10
F5	268.88 ± 3.60
F8	296.60 ± 1.08
Bz HCl pure drug	308.92 ± 2.47
F5 + Bz HCl	279.76 ± 3.97
PHB powder + Bz HCl	284.96 ± 1.23
F5 @Tumaker	292.85 ± 2.68
F5 + Bz HCl @Tumaker	290.10 ± 5.48
PHB powder @BIOX	290.24 ± 4.23
PHB powder + Bz HCl @BIOX	287.98 ± 3.00

3.3.3. Fourier-transform infrared spectroscopy (FTIR)

FTIR analysis was performed to investigate the structural characteristics of the samples, as well as to assess the presence of possible chemical interactions and uniform distribution of the drug within the formulations. The resulting spectra are illustrated in Fig. 6.

Raw materials: Only minor differences were detected among the various PHB forms (Fig. 6, panel I-A), all of which exhibited the typical absorption bands of the polymer described in the literature. An intense and sharp absorption band, characteristic of PHB, was observed at approximately 1721 cm^{-1}, which is attributed to the carbonyl (C=O) bond stretching vibration, as well as peaks at 1454 and 1381 cm^{-1}, attributed to aliphatic CH_2 and CH_3 groups, respectively and bands around 1290, 1282, 1184, and 1132 cm^{-1}, which are typical features of vibrations of the -C-O, -C-C-O, and C-O-C bonds in esters [56,57]. Differences between the PHB forms concerned the intensity of some signals and were more pronounced in the case of pellets. Pellets exhibited peaks around 1182, 1038, 733, and 452 cm^{-1}, that were absent or weak in the other PHB forms and that are due to the presence of additives, as also demonstrated by DSC and TGA analyses.

Drug and drug-loaded formulations: The FTIR spectra of drug-loaded formulations shown in Fig. 6-A and B, are very similar to those of corresponding unloaded forms with the only difference being the appearance of the characteristic peaks of the Bz HCl, confirming the presence of the drug within the formulations: the signals around 1527 cm^{-1} e 1496 cm^{-1} are related to C=C and C=N stretching, and the peaks at about 769 cm^{-1} and 745 cm^{-1} are attributed to aromatic C—H bending [58].

3D-printed scaffolds: The results are shown in Fig. 6-A and B and compared to those obtained for corresponding raw materials. No additional signals were detected, and no significant shifts detected, as also described by some researchers. The only slight differences observed were limited to intensity of absorption bands. Therefore, the structural and chemical integrity of the material after 3D-printing was confirmed.

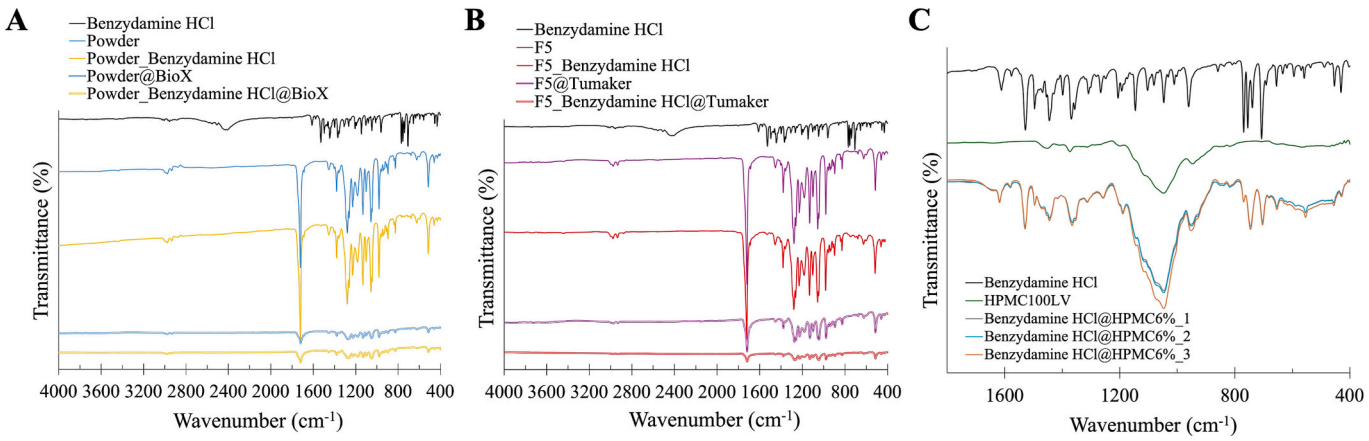

Fig. 6. FTIR spectra of raw materials, drug-loaded formulations and 3D-printed scaffolds (A-B); FTIR spectra of Bz HCl, HPMC and drug-loaded gel showing the homogeneous distribution of the drug.

3.3.4. Powder X-ray diffraction (PXRD)

The PXRD analysis was conducted to define the crystalline state of the samples.

Raw materials: The XRD patterns of the various forms of PHB (Fig. 7-A) exhibited several diffraction peaks that are characteristics of the orthorhombic structure of the polymer in the typical region of 2θ = 10–30°. Two strong and sharp reflection peaks were detected at 2θ values of 13.5° and 17°, corresponding to (020) and (110) planes of the orthorhombic unit cell, respectively [43,59]. The high intensity of these signals confirmed the presence of significant PHB fraction in crystalline state. A marked difference was observed between pellets and the other forms of PHB in terms of the intensity of diffraction peaks. Pellets exhibited weak reflection peaks, indicating a lower degree of crystallinity, while powder and granules displayed similar intensity patterns.

Drug and drug-loaded formulations: The results obtained are illustrated in Fig. 7-C and D. The Bz HCl-loaded powder blend showed a diffraction pattern characterized by both characteristic peaks of the polymer and typical signals of the drug. The latter had very intense reflections peaks at 2θ values of approximately 7.1°, 14.3°, 21.4°, 28.7° and 36° in agreement with literature [49] indicating the highly

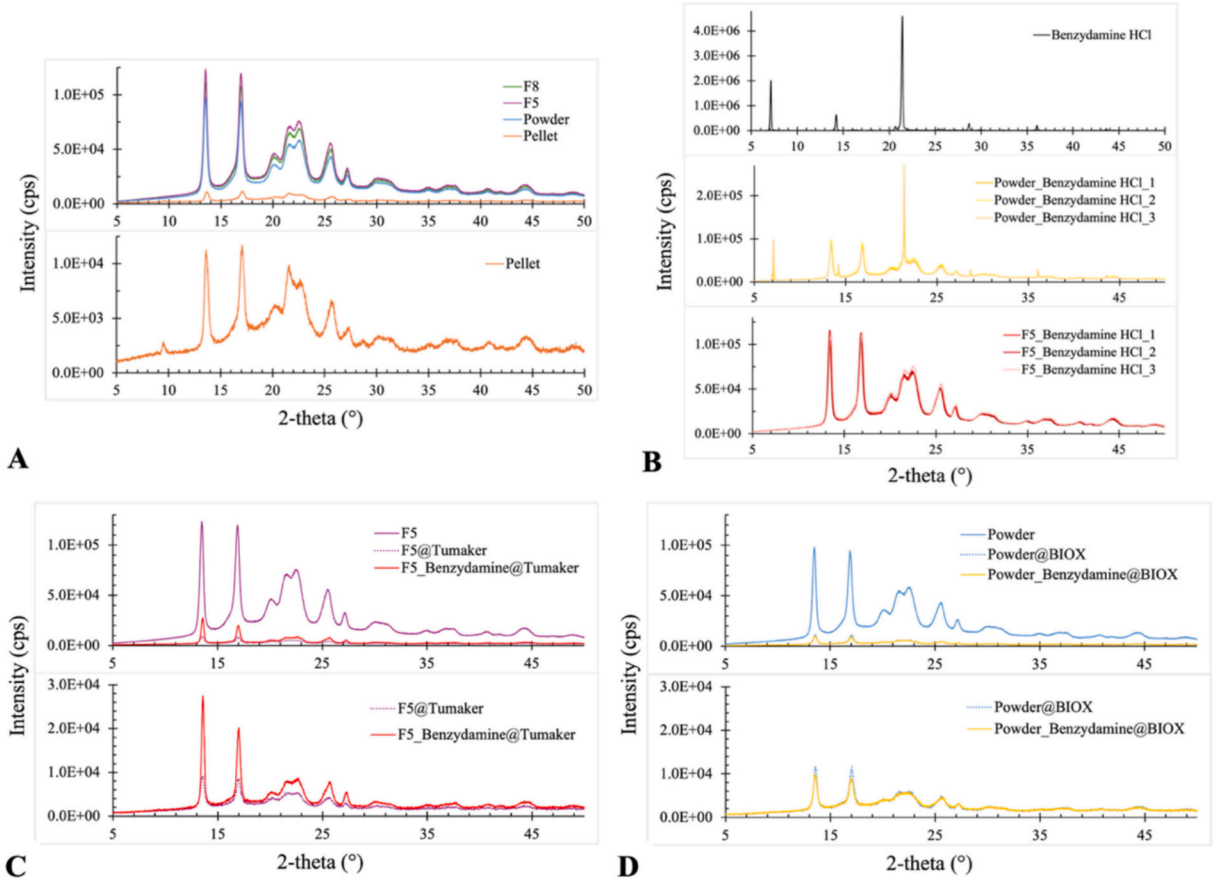

Fig. 7. PXRD diffractograms of raw materials, drug-loaded formulations and 3D-printed scaffolds. PXRD patterns of PHB powder, pellets and granules F5 and F8 (A); PXRD patterns of Bz HCl and drug-loaded formulations (B); PXRD patterns of 3D-printed scaffolds from unloaded and drug-loaded granules (C); PXRD patterns of 3D-printed scaffolds from free and drug-loaded powder (D).

crystalline nature of the drug (Fig. 7-B). Instead, the diffractogram of F5 granules containing the drug exhibited a very similar profile to that of unloaded granules, without the presence of characteristic peaks of Bz HCl. The absence of these signals suggested that after wet-granulation, the highly soluble drug is no longer detected in a crystalline phase in contrast to the powder blend, in which Bz HCl maintained its crystalline nature following physical blending with PHB. Furthermore, for both drug-loaded formulations, the diffractograms of three samples randomly collected from the same batch showed no differences in signal intensity (Fig. 7-B), confirming the homogeneity of the system in agreement with FTIR and HPLC results.

3D-printed scaffolds: The PXRD patterns of 3D-printed scaffolds (Fig. 7-C and D) were comparable to those of corresponding raw materials, displaying all the typical diffraction peaks of PHB. Only slight decreased intensity of each signal was found, indicating a reduction of the fraction of the polymer in the crystalline state after melting during the 3D printing process. Furthermore, the characteristic signals of the drug were not observed, especially for 3D-printed scaffolds from the powder blend, suggesting that Bz HCl, throughout the 3D-printing process is converted from a crystalline to an amorphous state with no evidence of subsequent recrystallization, in accordance also with DSC results reported in Section 3.3.1.

3.3.5. Scanning electron microscopy

The morphological features of the different samples were observed and investigated by employing scanning electron microscopy (SEM) and reported in Fig. 8.

Raw materials: SEM images highlighted clear morphological differences among the various forms of PHB. In the case of pellets (Fig. 8, panel I-A) a smooth and compact surface was revealed, while SEM images of powder (Fig. 8, panel I—B) and granules (Fig. 8, panel I—C and D) showed the high degree of crystallinity of PHB, with particles predominantly exhibiting a spheroidal shape. The main difference between powder and granules was observed in the particle compactness and

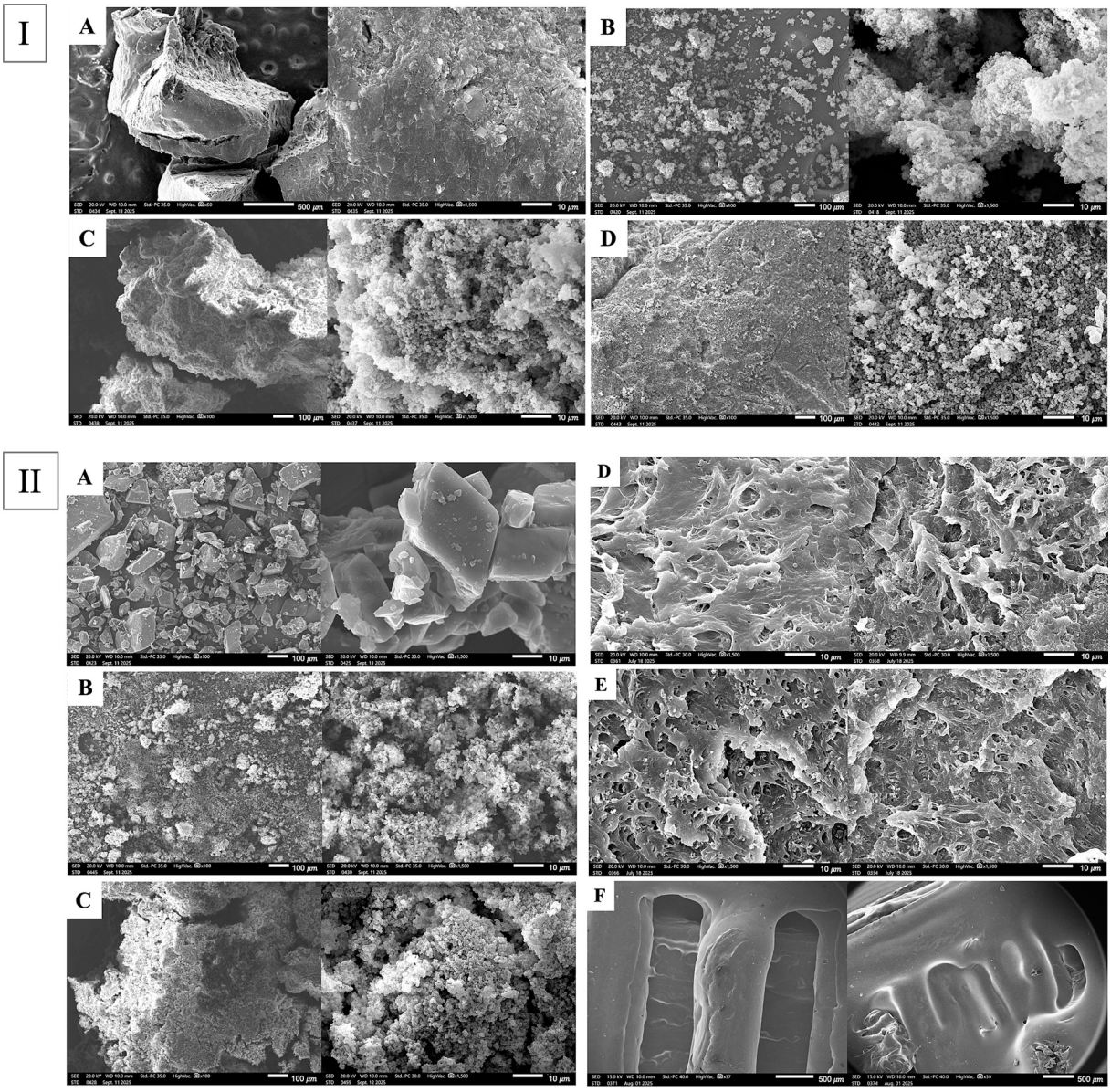

Fig. 8. SEM images of the various forms of PHB (Panel I); Bz HCl, drug-loaded formulations and 3D-printed products (Panel II). Panel I: A) pellets; B) powder; C) F5; D) F8. Panel II: A) Benzydamine hydrochloride; B) physical powder blend; C) drug-loaded granules F5; D) cross-section of 3D-printed scaffold from PHB free powder (on the left) and from physical powder blend (on the right); E) cross-section of 3D-printed scaffold from granules F5 (on the left) and from drug-loaded granules F5 (on the right); F) cross-section of 3D-printed final device without gel (on the left) and with gel (on the right).

organization: in the powder, aggregation was minimal, with only a limited number of particles interconnected, whereas the granules exhibited more compact and ordered aggregates. In particular, granules F5 displayed a more compact and regular internal organization compared with granules F8, that were characterized by poorly cohesive and disordered microstructures, partially resembling the morphological features of the powder.

Drug and drug-loaded formulations: SEM images of Bz HCl (Fig. 8, panel II-A) revealed large, rectangular-shaped crystals, confirming the high degree of crystallinity typical of the drug. Furthermore, SEM analysis of drug-loaded formulations (Fig. 8, panel II-B and C) displayed spheroidal particles and highlighted, in this case as well, differences in their degree of organization. Thus, drug-loading resulted in only minor morphological changes, with the physical powder blend exhibiting an overall more homogeneous and cohesive morphology than free PHB powder.

3D-printed scaffolds: SEM images of the cross-sectional areas of the various 3D-printed models, shown in Fig. 8, panel II-D and E, revealed no significant differences among the printed scaffolds. The internal structure appeared complex and homogeneous, with higher porosity observed in samples printed from granules. Considering the final 3D-printed device (Fig. 8, panel II-F), a smooth surface was observed, confirming a good level of accuracy in both the overall structure and the superposition of the deposited layers.

3.4. Drug content and uniformity of Bz HCl-loaded formulations

The uniform drug distribution within all Bz HCl-loaded formulations (PHB powder, granules F5 and HPMC gel) was evaluated.

Considering PHB formulations containing Bz HCl, the effective drug content was determined through a quantitative analysis (UV-HPLC) and the results obtained were referred to the theoretical API amount loaded in each sample. For F5 granules drug loading efficiency was 100.29% ± 2.84%, the powder exhibited a value of 97.64 ± 4.06%, and 98.65 ± 1.73% for the Bz HCl-loaded gel, showing no significant loss during the preparation of the two formulations. The homogeneous distribution of the drug was assessed, analysing three samples taken randomly from the system and evaluating the resulting area under the curve (AUC) of the corresponding chromatographic traces. The areas were found to be comparable with a relative standard deviation (RSD) $\leq$ 5% confirming a satisfactory homogeneous distribution of Bz HCl within blends.

For the same purpose, an FTIR analysis was performed on HPMC gel containing the drug. The resulting spectra are reported in Fig. 6, panel II-B and compared to those of HPMC and Bz HCl. Spectra showed the typical peaks of the HPMC, including signals in the range of 2969 cm^{-1} to 2821 cm^{-1} related to asymmetric and symmetric C—H vibrations and, in particular, the broadband at 1045 cm^{-1} attributed to C-O-C asymmetric stretching [30] and the characteristic peaks of the drug: signals at 1529 cm^{-1} and 1496 cm^{-1} assigned to C═C and C═N stretching and peaks in the range of 769 to 700 cm^{-1} corresponding to aromatic C—H bending [58]. The uniform distribution of Bz HCl within the gel was evaluated by analysing three portions of the gel and comparing the corresponding spectra. No significant variations in the intensity of the characteristic drug peaks were observed, demonstrating a homogeneous distribution of the drug within the prepared gel.

3.5. In vitro drug release

A dissolution study in phosphate-buffered saline PBS (pH = 7.4) was conducted to study the release profile of Bz HCl from the designed device, which consists of an external PHB matrix containing a HPMC gel (6% *w/v*). Each device presents a total mass of 73.27 ± 2.92 mg and a rectangular shape geometry, 9 × 4.5 × 2.5 mm. Specifically, the PHB-based portion has a mass of 59.65 ± 3.46 mg and thus an overall amount of ~1 mg of Bz HCl. On the other hand, the HPMC-based portion has a theoretical mass of ~20–25 mg (0.2 mL of gel deposited) thus a total of 3 mg of Bz HCl.

The results, reported in Fig. 9, confirmed a dual release pattern, closely associated with the composition and specific function of the two matrices constituting the system. Specifically, the release ratio of the drug from the gel matrix was relatively fast and immediate, with approximately 42.47 ± 4.72% released in 5 min and an almost complete release obtained within 6 h, as shown in Fig. 9-A. This release behaviour was indicative of a burst effect driven by the high hydrophilicity and high swelling capacity of the gel. The release profile of Bz HCl from the gel matrix was fitted with empirical mathematical models and the best fit (R^2 = 0.9921) was obtained for Korsmeyer-Peppas, suggesting a release mechanism predominantly governed by diffusion through the polymer matrix, which swelled upon hydration.

In contrast, the release of Bz HCl from the external PHB matrix was gradual and extremely slow, with only 3.31 ± 0.17% released after 4 days (Fig. 9-B). This outcome could be attributed to the physicochemical properties of PHB, which is characterized by prolonged degradation times [60,61]. Such properties hinder water penetration into the matrix and restrict the outward diffusion of the drug, making PHB a suitable material for controlled and sustained drug release.

While these release results were obtained at physiological pH (7.4), the in vitro profile is intended as a conservative reference, as drug release behaviour may vary under in vivo conditions. Minor transient pH fluctuations typical of the oral cavity (pH 6.2–7.6) are not expected to significantly affect the system, since PHB is a hydrophobic polyester with high hydrolytic stability, and its degradation and diffusion-driven release are likely influenced more by surface erosion and biological factors than by pH-dependent hydrolysis. Thus, under clinical conditions, interactions with the oral environment, including enzymatic and microbiological activity, may therefore contribute to scaffold erosion and potentially increase release kinetics, while preserving structural integrity and delivery robustness.

3.6. In vitro antimicrobial activity

According to literature data, Bz HCl has been reported to exhibit antimicrobial activity against several common oral pathogens, including *Staphylococcus aureus* and *Candida albicans,* with minimum inhibitory concentration (MIC) values of 554 μg/mL and 277 μg/mL, respectively, and a minimum bactericidal concentration (MBC) of 554 μg/mL for both pathogens [49]. Thus, considering that the developed device (average weight of approximately 75 mg) contained ~4 mg of Bz HCl (~ 3 mg and ~ 1 mg in the immediate and controlled release portions, respectively), and based on the drug release profiles, an effective antimicrobial activity against these pathogens could be reasonably expected.

The results of the preliminary antimicrobial studies are shown in Fig. 10. A well-defined zone of microbial growth inhibition was observed. Since the device does not have a circular geometry, the inhibition area was elliptical, and both the major and minor axes were measured. For *Staphylococcus aureus*, the major and minor axes were 1.8 cm and 1.5 cm, respectively, with a distance from the device of approximately 0.5 cm. In the case of *Candida albicans*, a slightly lower inhibition effect was observed, with major and minor axes measuring 1.5 cm and 1.3 cm, respectively, and distance of about 0.4 cm. It is important to acknowledge that the static antimicrobial assay used here does not fully reproduce the dynamic oral environment, where continuous salivary flow can dilute or remove topically applied agents. However, the delivery system evaluated in the present study is intended to function within the confined space between the aligner and the mucosa, where fluid turnover is substantially lower than in the open oral cavity. This localized micro-environment reduces the "wash-out" effect and allows the released drug to remain in contact with the mucosa for longer periods. Within this context, the immediate release from the HPMC gel is designed to rapidly saturate the enclosed space, while the slower release from the PHB scaffold helps maintain local concentrations over time. Overall, the achieved results suggested the therapeutic potential of the

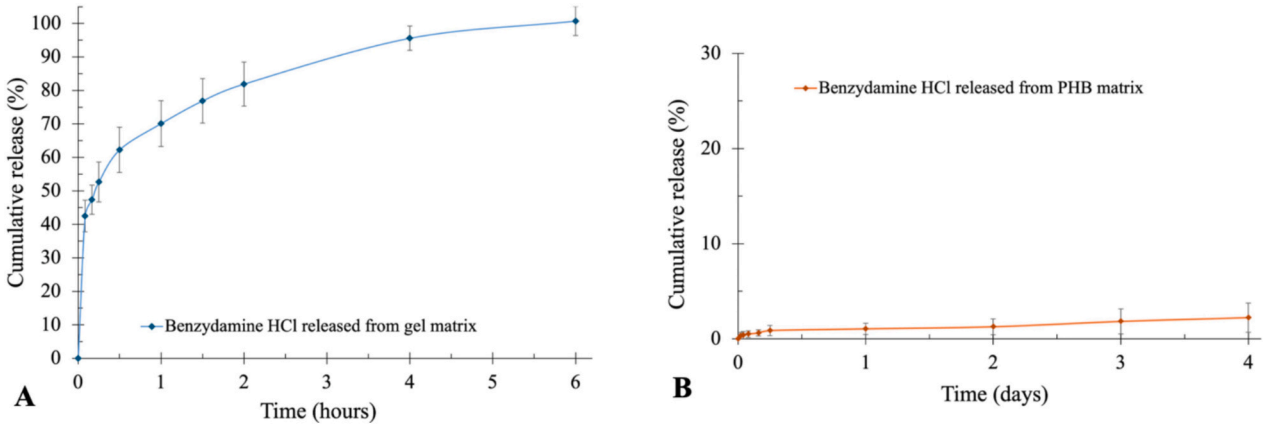

Fig. 9. Release profile of Bz HCl from gel matrix (A) and from external PHB matrix (B).

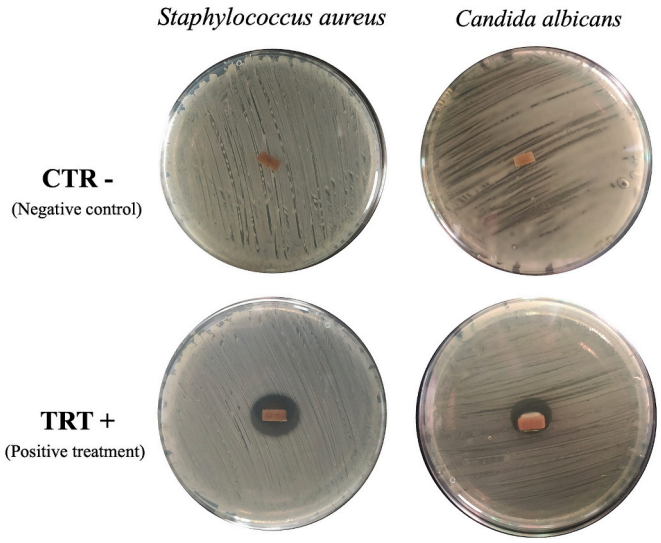

Fig. 10. Antibacterial activity of the 3D-printed Bz HCl-loaded scaffolds against *S. aureus* and *C. albicans* compared to the control. Microbial growth inhibition was observed only in the presence of drug-loaded device (CRT +), while the unloaded device was used as the negative control (CTR-).

drug-loaded device, which demonstrated its capability of controlling the proliferation of pathogenic bacteria and fungi.

4. Conclusion

This study demonstrates the feasibility and potential of integrating polyhydroxybutyrate (PHB) into additive manufacturing, with a particular focus on direct powder extrusion 3D printing. A comprehensive characterization of PHB in different starting forms was performed, providing insight into its processability and suitability for this manufacturing approach. In addition, a proof-of-concept medical device based on PHB was developed, highlighting its potential for dual drug release in dental applications. Overall, these findings could facilitate the wider adoption of PHB across diverse applications, advancing green manufacturing technologies. By demonstrating the feasibility of PHB in 3D printing, this research supports the development of sustainable materials and contributes to the shift towards a circular economy. Successful integration of PHB into additive manufacturing may enable the production of eco-friendly products with a reduced environmental footprint, aligning with global sustainability objectives. The integration of bio-sourced polymers such as PHB with DPE technology represents a synergistic approach towards green manufacturing, reducing both material-related environmental impact and processing energy requirements. Furthermore, the use of PHB in biomedical applications, such as drug delivery devices and dental implants, highlights its versatility and potential to improve patient outcomes while minimizing ecological impact. Continued research and optimization of PHB processing will be crucial to unlock its full potential in industrial and clinical settings, fostering innovation in both sustainability and healthcare sectors.

CRediT authorship contribution statement

Costanza Fratini: Methodology, Investigation, Formal analysis, Data curation, Writing – original draft. **Matteo Grandoni:** Investigation, Formal analysis, Data curation, Writing – original draft. **Tania Vanzolini:** Methodology, Investigation, Formal analysis, Data curation, Writing – original draft. **Annalisa Aluigi:** Data curation, Writing – review & editing. **Mattia Tiboni:** Data curation, Writing – review & editing. **Luca Casettari:** Supervision, Resources, Project administration, Conceptualization, Writing – review & editing.

Funding

This work has been funded by the European Union - NextGenerationEU, Mission 4, Component 2, under the Italian Ministry of University and Research (MUR) National Innovation Ecosystem grant ECS00000041 - VITALITY – CUP H33C22000430006.

Declaration of competing interest

The authors declare that they have no known competing financial interests or personal relationships that could have appeared to influence the work reported in this paper.

Acknowledgments

The authors would like to thank 3D Objects & Data Software SA (Switzerland) for providing the dental aligners (Donatello Aligners). The authors gratefully acknowledge Ilaria Marinelli for the technical assistance and support provided during the experimental work.

Data availability

Data will be made available on request.

References

[1] A. Anjum, M. Zuber, K.M. Zia, A. Noreen, M.N. Anjum, S. Tabasum, Microbial production of polyhydroxyalkanoates (PHAs) and its copolymers: a review of

recent advancements, Int. J. Biol. Macromol. 89 (2016) 161–174, https://doi.org/10.1016/j.ijbiomac.2016.04.069.
[2] A. Steinbüchel, T. Lütke-Eversloh, Metabolic engineering and pathway construction for biotechnological production of relevant polyhydroxyalkanoates in microorganisms, Biochem. Eng. J. 16 (2003) 81–96, https://doi.org/10.1016/S1369-703X(03)00036-6.
[3] S. Jha, T. Pandaya, A review on Polyhydroxybutyrate (PHB): production, properties, applications, and environmental implications, International Journal of Novel Research and Development 9 (2024) 277–288. https://ijnrd.org/papers/IJNRD2404734.pdf.
[4] A.Z. Naser, I. Deiab, F. Defersha, S. Yang, Expanding poly(lactic acid) (pla) and polyhydroxyalkanoates (phas) applications: a review on modifications and effects, Polymers (Basel). 13 (2021), https://doi.org/10.3390/polym13234271.
[5] J. Żur-Pińska, M.Z. Gładysz, D. Ubels, J. Siebring, M.K. Włodarczyk-Biegun, Smart and sustainable: exploring the future of PHAs biopolymers for 3D printing in tissue engineering, Sustain. Mater. Technol. 38 (2023), https://doi.org/10.1016/j.susmat.2023.e00750.
[6] J. Zhang, E.I. Shishatskaya, T.G. Volova, L.F. da Silva, G.Q. Chen, Polyhydroxyalkanoates (PHA) for therapeutic applications, Mater. Sci. Eng. C 86 (2018) 144–150, https://doi.org/10.1016/j.msec.2017.12.035.
[7] A.A. Barmpaki, U.C. Paul, M. Nardi, A. Athanassiou, Eco-friendly blends of polylactic acid and polyhydroxybutyrate enhanced with epoxidized soybean oil methyl ester for food-packaging applications, ACS Appl. Polym. Mater. 6 (2024) 8997–9007, https://doi.org/10.1021/acsapm.4c01341.
[8] P. Prakash, W.H. Lee, H.S.J. Ching-Yeeloo, T. Parumasivam Wong, Advances in polyhydroxyalkanoate nanocarriers for effective drug delivery: an overview and challenges, Nanomaterials 12 (2022), https://doi.org/10.3390/nano12010175.
[9] M. Mehrpouya, H. Vahabi, M. Barletta, P. Laheurte, V. Langlois, Additive manufacturing of polyhydroxyalkanoates (PHAs) biopolymers: materials, printing techniques, and applications, Mater. Sci. Eng. C 127 (2021), https://doi.org/10.1016/j.msec.2021.112216.
[10] A. Kovalcik, Recent advances in 3D printing of polyhydroxyalkanoates: a review, Eur. J. Dermatol. 5 (2021) 48–55, https://doi.org/10.2478/ebtj-2021-0008.
[11] V.M. Vaz, L. Kumar, 3D printing as a promising tool in personalized medicine, AAPS Pharm Sci Tech 22 (2021), https://doi.org/10.1208/s12249-020-01905-8.
[12] W. Jamróz, J. Szafraniec, M. Kurek, R. Jachowicz, 3D printing in pharmaceutical and medical applications – recent achievements and challenges, Pharm. Res. 35 (2018), https://doi.org/10.1007/s11095-018-2454-x.
[13] J. Bernatoniene, J. Stabrauskiene, J.A. Kazlauskaite, U. Bernatonyte, D. M. Kopustinskiene, The future of medicine: how 3D printing is transforming pharmaceuticals, Pharmaceutics 17 (2025), https://doi.org/10.3390/pharmaceutics17030390.
[14] S. Wang, X. Chen, X. Han, X. Hong, X. Li, H. Zhang, M. Li, Z. Wang, A. Zheng, A review of 3D printing technology in pharmaceutics: technology and applications, now and future, Pharmaceutics 15 (2023), https://doi.org/10.3390/pharmaceutics15020416.
[15] S. Moroni, S. Khorshid, A. Aluigi, M. Tiboni, L. Casettari, Poly(3-hydroxybutyrate): a potential biodegradable excipient for direct 3D printing of pharmaceuticals, Int. J. Pharm. 623 (2022), https://doi.org/10.1016/j.ijpharm.2022.121960.
[16] R. Yahyapour, Y.Z. Menceloglu, Blending strategies for green packaging: enhancing polyhydroxybutyrate performance for sustainable solutions, Eur. Polym. J. 228 (2025), https://doi.org/10.1016/j.eurpolymj.2025.113821.
[17] W. Crupano, B. Adrover-Monserrat, J. Llumà, R. Jerez-Mesa, J.A. Travieso-Rodriguez, Investigating mechanical properties of 3D printed polylactic acid/poly-3-hydroxybutyrate composites. Compressive and fatigue performance, Heliyon 10 (2024), https://doi.org/10.1016/j.heliyon.2024.e38066.
[18] A.A. Vaidya, C. Collet, M. Gaugler, G. Lloyd-Jones, Integrating softwood biorefinery lignin into polyhydroxybutyrate composites and application in 3D printing, Mater. Today Commun. 19 (2019) 286–296, https://doi.org/10.1016/j.mtcomm.2019.02.008.
[19] M. Zhang, N.L. Thomas, Blending polylactic acid with polyhydroxybutyrate: the effect on thermal, mechanical, and biodegradation properties, Adv. Polym. Technol. 30 (2011) 67–79, https://doi.org/10.1002/adv.20235.
[20] J. Yang, B. Sun, J. Dai, X. Li, Y. Zhao, L. Zhang, J. Bai, F. Xue, C. Chu, Design and fabrication of durable poly(3-hydroxybutyrate) (PHB) coating with high adhesion and desirable anti-corrosion performance on Mg alloy for bio-application, Prog. Org. Coat. 194 (2024), https://doi.org/10.1016/j.porgcoat.2024.108577.
[21] A. Giubilini, M. Messori, F. Bondioli, P. Minetola, L. Iuliano, G. Nyström, K. Maniura-Weber, M. Rottmar, G. Siqueira, 3D-printed poly(3-hydroxybutyrate-co-3-hydroxyhexanoate)-cellulose-based scaffolds for biomedical applications, Biomacromolecules 24 (2023) 3961–3971, https://doi.org/10.1021/acs.biomac.3c00263.
[22] G. Pecorini, M.A.N. Domingos, S.M. Richardson, L. Carmassi, D.L. Vecchi, G. Parrini, D. Puppi, 3D printing of bacterial poly(3-hydroxybutyrate-co-3-hydroxyvalerate)/poly(lactide-co-glycolide) blend loaded with β-tricalcium phosphate for the development of scaffolds to support human mesenchymal stromal cell proliferation, Int. J. Biol. Macromol. 288 (2025), https://doi.org/10.1016/j.ijbiomac.2024.138744.
[23] V. Melčová, Š. Krobot, J. Šindelář, E. Šebová, M.K. Rampichová, R. Přikryl, The effect of surface roughness and wettability on the adhesion and proliferation of Saos-2 cells seeded on 3D printed poly(3-hydroxybutyrate)/polylactide (PHB/PLA) surfaces, Results Surf. Interfaces 16 (2024), https://doi.org/10.1016/j.rsurfi.2024.100271.
[24] M. Fanous, S. Gold, S. Hirsch, J. Ogorka, G. Imanidis, Development of immediate release (IR) 3D-printed oral dosage forms with focus on industrial relevance, Eur. J. Pharm. Sci. 155 (2020), https://doi.org/10.1016/j.ejps.2020.105558.
[25] A. Goyanes, N. Allahham, S.J. Trenfield, E. Stoyanov, S. Gaisford, A.W. Basit, Direct powder extrusion 3D printing: fabrication of drug products using a novel single-step process, Int. J. Pharm. 567 (2019), https://doi.org/10.1016/j.ijpharm.2019.118471.
[26] M. Rouzi, X. Zhang, Q. Jiang, H. Long, W. Lai, X. Li, Impact of clear aligners on Oral health and Oral microbiome during orthodontic treatment, Int. Dent. J. 73 (2023) 603–611, https://doi.org/10.1016/j.identj.2023.03.012.
[27] A. Ferrer-Montiel, Benzydamine hydrochloride: an overview on a well-established drug with news in mechanisms of action, F1000Res 13 (2024) 350, https://doi.org/10.12688/f1000research.144067.1.
[28] M.D. Arpa, A.P. Yağcılar, S.N. Biltekin, Novel benzydamine hydrochloride and chlorhexidine gluconate loaded bioadhesive films for local treatment of buccal infections, J. Drug Delivery Sci. Technol. 84 (2023), https://doi.org/10.1016/j.jddst.2023.104497.
[29] A. Ardizzoni, G. Boaretto, E. Pericolini, D. Pinetti, A. Capezzone de Joannon, L. Durando, L. Ragni, E. Blasi, Effects of benzydamine and mouthwashes containing benzydamine on Candida albicans adhesion, biofilm formation, regrowth, and persistence, Clin. Oral Investig. 26 (2022) 3613–3625, https://doi.org/10.1007/s00784-021-04330-8.
[30] C. Fratini, S. Moroni, D. De Angelis, M. Tiboni, A.G. Balducci, A. Rossi, A. Aluigi, F. Amadei, L. Casettari, Direct powder extrusion (DPE) 3D-printing of mini-tablets for preclinical studies in rodents, Int. J. Pharm. 675 (2025), https://doi.org/10.1016/j.ijpharm.2025.125542.
[31] S.A. Sánchez-Guirales, N. Jurado, A. Kara, A. Lalatsa, D.R. Serrano, Understanding direct powder extrusion for fabrication of 3d printed personalised medicines: a case study for nifedipine minitablets, Pharmaceutics 13 (2021), https://doi.org/10.3390/pharmaceutics13101583.
[32] W. Kanabenja, N. Passornraprasit, C. Aumnate, T.A. Osswald, D. Aht-Ong, P. Potiyaraj, Enhancing 3D printability of polyhydroxybutyrate (PHB) and poly(3-hydroxybutyrate-co-3-hydroxy valerate) (PHBV) based blends through melt extrusion based-3D printing, Addit. Manuf. 86 (2024), https://doi.org/10.1016/j.addma.2024.104205.
[33] L. Lendvai, I. Fekete, D. Rigotti, A. Pegoretti, Experimental study on the effect of filament-extrusion rate on the structural, mechanical and thermal properties of material extrusion 3D-printed polylactic acid (PLA) products, Prog. Addit. Manuf. 10 (2025) 619–629, https://doi.org/10.1007/s40964-024-00646-5.
[34] F. Tikhani, A. Gurbin, P. Hubert, Unveiling the impact of short fibre reinforcement and extrusion properties on microstructure of 3D printed polycarbonate composites, Addit. Manuf. 93 (2024), https://doi.org/10.1016/j.addma.2024.104423.
[35] S. Kontárová, R. Přikryl, V. Melčová, P. Menčík, M. Horálek, S. Figalla, R. Plavec, J. Feranc, J. Sadílek, A. Pospíšilová, Printability, mechanical and thermal properties of poly(3-hydroxybutyrate)-poly(lactic acid)-plasticizer blends for three-dimensional (3D) printing, Materials 13 (2020) 1–28, https://doi.org/10.3390/ma13214736.
[36] F. Laoutid, H. Lenoir, A. Molins Santaeularia, A. Toncheva, T. Schouw, P. Dubois, Impact-resistant poly(3-Hydroxybutyrate)/poly(ε-Caprolactone)-based materials, through reactive melt processing, for compression-molding and 3D-printing applications, Materials 15 (2022), https://doi.org/10.3390/ma15228233.
[37] M. Amir, S.F. Rizvi, M. Asif, A. Ahmad, M.B. Alshammari, A. Gupta, M.R. Zaheer, R. Roohi, Polyhydroxybutyrate (PHB) bioplastic characterization from the isolate pseudomonas stutzeri PSB1 synthesized using potato peel feedstock to combat solid waste management, Biocatal. Agric. Biotechnol. 57 (2024), https://doi.org/10.1016/j.bcab.2024.103097.
[38] C. Chen, X. Zhou, Y. Zhuang, L. Dong, Thermal behavior and intermolecular interactions in blends of poly(3-hydroxybutyrate) and maleated poly(3-hydroxybutyrate) with chitosan, J. Polym. Sci. B 43 (2005) 35–47, https://doi.org/10.1002/polb.10742.
[39] M. Seggiani, P. Cinelli, S. Verstichel, M. Puccini, S. Vitolo, I. Anguillesi, A. Lazzeri, Development of fibres-reinforced biodegradable composites, Chem. Eng. Trans. 43 (2015) 1813–1818, https://doi.org/10.3303/CET1543303.
[40] N. Follain, C. Chappey, E. Dargent, F. Chivrac, R. Crétois, S. Marais, Structure and barrier properties of biodegradable polyhydroxyalkanoate films, J. Phys. Chem. C 118 (2014) 6165–6177, https://doi.org/10.1021/jp408150k.
[41] N.G. Jaques, I.D. Dos Santos Silva, M. Da Cruz Barbosa, A. Neto, E.L. Ries, R.M.R. Wellen Canedo, Effect of heat cycling on melting and crystallization of PHB/TiO2 compounds, Polimeros 28 (2018) 161–168, https://doi.org/10.1590/0104-1428.12416.
[42] Y.M. Corre, S. Bruzaud, J.L. Audic, Y. Grohens, Morphology and functional properties of commercial polyhydroxyalkanoates: a comprehensive and comparative study, Polym. Test. 31 (2012) 226–235, https://doi.org/10.1016/j.polymertesting.2011.11.002.
[43] R.R. de Sousa Junior, C.A.S. dos Santos, N.M. Ito, A.N. Suqueira, M. Lackner, D. J. dos Santos, PHB Processability and property improvement with linear-chain polyester oligomers used as plasticizers, Polymers (Basel). 14 (2022), https://doi.org/10.3390/polym14194197.
[44] M.A. Abdelwahab, A. Flynn, B. Sen Chiou, S. Imam, W. Orts, E. Chiellini, Thermal, mechanical and morphological characterization of plasticized PLA-PHB blends, Polym. Degrad. Stab. 97 (2012) 1822–1828, https://doi.org/10.1016/j.polymdegradstab.2012.05.036.
[45] L. Perioli, V. Ambrogi, C. Pagano, E. Massetti, C. Rossi, New solid mucoadhesive systems for benzydamine vaginal administration, Colloids Surf. B Biointerfaces 84 (2011) 413–420, https://doi.org/10.1016/j.colsurfb.2011.01.035.
[46] J. Elbl, J. Gajdziok, J. Kolarczyk, 3D printing of multilayered orodispersible films with in-process drying, Int. J. Pharm. 575 (2020), https://doi.org/10.1016/j.ijpharm.2019.118883.

[47] P. Main, S. Petersmann, N. Wild, M. Feuchter, I. Duretek, M. Edeleva, P. Ragaert, L. Cardon, T. Lucyshyn, Impact of multiple reprocessing on properties of polyhydroxybutyrate and polypropylene, Polymers (Basel). 15 (2023), https://doi.org/10.3390/polym15204126.
[48] L.F. Rivas, S.A. Casarin, N.C. Nepomuceno, M.I. Alencar, J.A.M. Agnelli, E.S. De Medeiros, A. De Oliveira Wanderley Neto, M.P. De Oliveira, A.M. De Medeiros, A.S. Ferreira Santos, Reprocessability of PHB in extrusion: ATR-FTIR, tensile tests and thermal studies, Polimeros 27 (2017) 122–128, https://doi.org/10.1590/0104-1428.2406.
[49] M. Mehravaran, A. Haeri, S. Rabbani, S.A. Mortazavi, M. Torshabi, Preparation and characterization of benzydamine hydrochloride-loaded lyophilized mucoadhesive wafers for the treatment of oral mucositis, J. Drug Delivery Sci. Technol. 78 (2022), https://doi.org/10.1016/j.jddst.2022.103944.
[50] L. Dan, Q. Cheng, R. Narain, B. Krause, P. Pötschke, A. Elias, Three-dimensional printed and biocompatible conductive composites comprised of Polyhydroxybutyrate and multiwalled carbon nanotubes, Ind. Eng. Chem. Res. 60 (2021) 885–897, https://doi.org/10.1021/acs.iecr.0c04753.
[51] S. Weinmann, C. Bonten, Thermal and rheological properties of modified polyhydroxybutyrate (PHB), Polym. Eng. Sci. 59 (2019) 1057–1064, https://doi.org/10.1002/pen.25075.
[52] A.J. dos Santos, L.V. Oliveira Dalla Valentina, A.A. Hidalgo Schulz, M.A. Tomaz Duarte, From obtaining to degradation of PHB: a literature review, Part II, Ing. Cienc. 14 (2018) 207–228, https://doi.org/10.17230/ingciencia.14.27.9.
[53] H. Ariffin, H. Nishida, Y. Shirai, M.A. Hassan, Determination of multiple thermal degradation mechanisms of poly(3-hydroxybutyrate), Polym. Degrad. Stab. 93 (2008) 1433–1439, https://doi.org/10.1016/j.polymdegradstab.2008.05.020.
[54] S.D. Li, J.D. He, P.H. Yu, M.K. Cheung, Thermal degradation of poly(3-hydroxybutyrate) and poly(3-hydroxybutyrate-co-3-hydroxyvalerate) as studied by TG, TG-FTIR, and Py-GC/MS, J. Appl. Polym. Sci. 89 (2003) 1530–1536, https://doi.org/10.1002/app.12249.
[55] A. Uda, H. Sato, Y. Ozaki, Melting/crystallization mechanism of biodegradable polymer, poly(3-hydroxybutyrate), studied by quantification of temperature-dependent IR spectra by nonlinear deconvolution, Spectrochim. Acta A Mol. Biomol. Spectrosc. 329 (2025), https://doi.org/10.1016/j.saa.2024.125576.
[56] D.A. Miranda, K. Marín, O. Sundman, M. Hedenström, J. Quillaguaman, A. Gorzsás, M. Broström, M. Carlborg, J. Lundqvist, L. Romero-Soto, L.J. Jönsson, C. Carrasco, C. Martín, Production and characterization of poly(3-hydroxybutyrate) from Halomonas boliviensis LC1 cultivated in hydrolysates of quinoa stalks, Fermentation 9 (2023), https://doi.org/10.3390/fermentation9060556.
[57] C. Trakunjae, A. Boondaeng, W. Apiwatanapiwat, A. Kosugi, T. Arai, K. Sudesh, P. Vaithanomsat, Enhanced polyhydroxybutyrate (PHB) production by newly isolated rare actinomycetes Rhodococcus sp. strain BSRT1-1 using response surface methodology, Sci. Rep. 11 (2021), https://doi.org/10.1038/s41598-021-81386-2.
[58] W. Samprasit, P. Opanasopit, B. Chamsai, Development and evaluation of Benzydamine hydrochloride-loaded pastilles for local delivery in the Oral cavity, J. Pharm. Innov. 20 (2025), https://doi.org/10.1007/s12247-025-10044-1.
[59] A.N. Frone, C.A. Nicolae, M.C. Eremia, V. Tofan, M. Ghiurea, I. Chiulan, E. Radu, C. M. Damian, D.M. Panaitescu, Low molecular weight and polymeric modifiers as toughening agents in poly(3-hydroxybutyrate) films, Polymers (Basel). 12 (2020) 1–20, https://doi.org/10.3390/polym12112446.
[60] V. Kundrat, N. Cernekova, A. Kovalcik, V. Enev, I. Marova, Drug release kinetics of electrospun PHB meshes, Materials 12 (2019), https://doi.org/10.3390/ma12121924.
[61] C. Villegas, A. Torres, J. Bruna, M.I. Bustos, A. Díaz-Barrera, J. Romero, A. Rojas, A. Guarda, Obtaining active polylactide (Pla) and polyhydroxybutyrate (phb) blends based bionanocomposites modified with graphene oxide and supercritical carbon dioxide (scco2)-assisted cinnamaldehyde: effect on thermal-mechanical, disintegration and mass transport properties, Polymers (Basel). 13 (2021), https://doi.org/10.3390/polym13223968.